UNIVERSITY OF CALIFORNIA
SANTA CRUZ

DYNAMICS OF INVERSE MAGNETIC BILLIARDS ON POLYGONS

A dissertation submitted in partial satisfaction of the
requirements for the degree of

DOCTOR OF PHILOSOPHY

in

MATHEMATICS

by

Andres Perico

June 2022

The Dissertation of Andres Perico
is approved:

Professor Richard Montgomery, Chair

Professor Francois Monard

Professor Longzhi Lin

Peter F. Biehl
Vice Provost and Dean of Graduate Studies

Contents

List of Figures

Abstract

Dynamics of Inverse Magnetic Billiards on Polygons

by

Andres Perico

We consider a polygon in a two-dimensional plane with a magnetic field orthogonal to the plane. The field is zero inside the polygon, and a nonzero constant outside. We study the dynamics of a particle with a negative charge moving on the plane under the influence of the field. Outside the polygon, it moves along arcs of circles going counterclockwise. Inside, it moves along line segments. The segments and arcs are joined at the polygonal boundary so that the velocity varies continuously. Problems arise because we have a boundary with corners, being this a significant obstacle for integrability. When the table is a square, we generalize some cases with rational velocities using symbolic dynamics. We also show numerical evidence of a chaotic-like behavior with other initial conditions; specifically, we use numerical methods to calculate the Lyapunov exponent for different settings of the dynamical billiard. We find 4.2 a similar, yet distant, result from [VTCP03], where the exponent heavily depends on the strength of the magnetic field. Our main results are a partial classification of the periodic orbits (section 3.2), and a strong numerical evidence that the map is chaotic and ergodic (section 4).

Keywords. Billiards, Magnetic, Inverse-magnetic, Chaotic, Sturmian sequences, Lyapunov exponent. **MSC2010.** 37J30, 37M05, 37M25, 70H99.

Acknowledgments

I have to thank first and foremost Laura and Luffy. For putting up with all my particularities, while doing, enduring, and excelling on the same path I was following; and for giving me a reason to keep going together every day. They are the reason I move forward every day.

I would like to thank Professor Richard Montgomery for his wisdom in math and life. I get smarter after every talk we have. He has guided me personally and professionally during these years in Santa Cruz.

I am also thankful to my math peers Vic, Erman, and Deniz; my math siblings Sean, Gabe, Steven, and Alejandro. They provided company and wisdom in my life as a Ph.D. student.

Lastly, I would not be here if it was not for my parents and sister, who sacrificed a lot to give me the best opportunities to succeed with my personal goals.

Chapter 1

Introduction

A dynamical billiard is a dynamical system that studies a particle inside a region Ω, when the particle hits the boundary $\partial\Omega$, it bounces off it according to some established rules.

The most common rules are the ones used in optics, acoustics, etc., where the angle of incidence is the same as the angle of reflection on $\partial\Omega$, and inside Ω, the particle moves on straight lines; with these specific rules the dynamical system is known as a "classical" billiard, if the boundary $\partial\Omega$ is smooth, the system is called a "Birkhoff" billiard.

Changing some rules and conditions of the system, mathematicians have been studying new dynamical billiards, like "magnetic" (with a magnetic field inside), "outer" (where the particle bounces outside Ω), and recently "symplectic" [AT18]. In this manuscript, we are going to study a variant that was first studied (and named) in physics [VTCP03], the "Inverse Magnetic" billiard. We concentrate on the case where Ω is a polygon.

The general concept of a dynamical billiard flow has two interpretations, a continuous trajectory and a discrete map between boundary points. In this chapter, we introduce the dynamical system 1.1.2, or continuous interpretation. In chapter

2.1, we introduce the billiard map - something that lets us use symbolic dynamics to study our system when the table is a square.

1.1 Setup

Consider $\Omega \subset \mathbb{R}^2$ a bounded, convex region on the plane, and B a piece-wise homogeneous magnetic field perpendicular to $\mathbb{R}^2$ defined by

$$B = B(q) = \begin{cases} 0, & q \in \Omega \\ B, & q \notin \Omega \end{cases} \tag{1.1.1}$$

Notice that inside Ω, there is no magnetic field. If we denote $\mathbb{J} := \begin{pmatrix} 0 & -1 \\ 1 & 0 \end{pmatrix}$ as a rotation counterclockwise by $\frac{\pi}{2}$, the ordinary differential equation that describe the motion of the particle is

$$\ddot{q} = B(q)\mathbb{J}\dot{q} \tag{1.1.2}$$

or

$$\begin{cases} \dot{q} = v \\ \dot{v} = B(q)\mathbb{J}v \end{cases}$$

A particle with charge e, mass m and speed $|v| = |\dot{q}|$ will move along circles of 'Larmor radius' $r = \frac{m|v|}{|eB|}$ outside Ω and on straight lines with velocity v inside Ω. The resulting dynamical system is called *inverse magnetic billiard*, first mentioned in [VTCP03]. A solution to 1.1.2 is called a billiard trajectory. This gives us the continuous interpretation of the dynamical billiard.

We insist that the trajectory is differentiable as it travels across the boundary $\partial\Omega$. As a result, we get a map much like the classical billiard map on the space of pairs (point on $\partial\Omega$, inward-pointing velocity vector), which is defined almost everywhere. Our goal is to understand this map and its dynamic properties when Ω is a polygon, especially when Ω is a square.

1.2 Some History

Mathematical standard billiards is a famous subject with many open problems ([Tab95] [KT91]). Magnetic billiards have been studied since 1985 ([RB85]), here, you have a constant magnetic field inside your billiard table, and your particle has a charge. In the next decade, this subject was explored in more detail ([BK96]).

Inverse magnetic billiards has not been studied thoroughly, as many mathematical subjects, physics studied first (condensed matter) under some experiments with pieces wise constant magnetic fields outside a set. A numerical study and history of this type of billiards can be found in ([VTCP03]). They studied the Bunimovich billiard [Bun07, Bun79], the famous stadium shape billiard. They use numerical methods to find a smooth transition from chaos to integrable, depending on the strength of the magnetic field B.

During the 1980s and 1990s, detecting and quantifying chaos was a favored problem in different subjects (medicine [FLN$^+$90], economics [Che88], physics [RCD93]). The popularity was partially thanks to methods developed to calculate Kolmogorov entropy [GP83], and Lyapunov exponents [WSSV85, SS85]. These two measures estimate the level of chaos in the dynamical system. After the years, the calculation methods have been optimized, but the essentials remain

the same. We follow [WSSV85] and [VTCP03] to find the Lyapunov Exponent for the inverse magnetic case.

1.3 Main results

Our main results can be divided into two categories, depending on if the particle's trajectory goes around a corner or not. See Figure 1.1. The methods used for studying the first category were not suitable for studying the second. The turning of corners appears to be the main mechanism leading to chaos in the system.

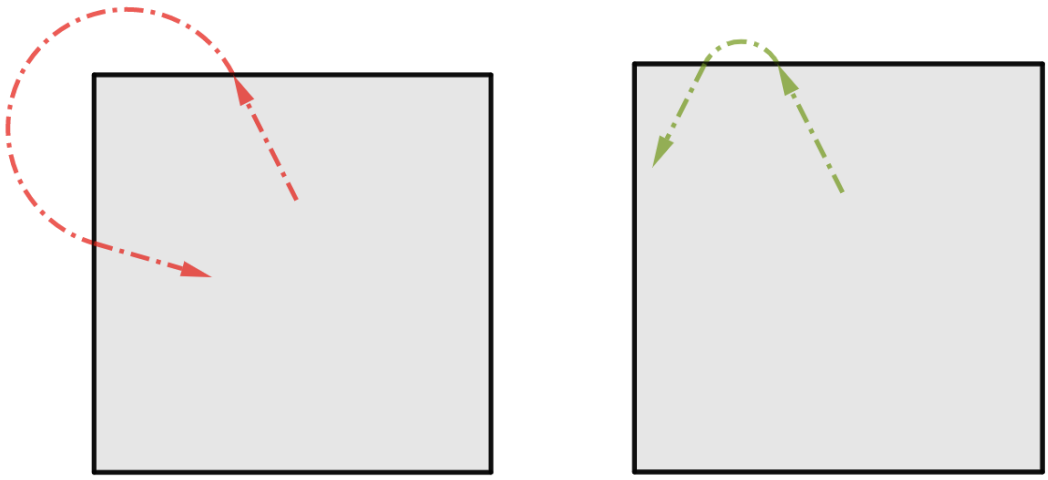

(a) Going around a corner **(b)** Not going around a corner

Figure 1.1: A particle on the Inverse Magnetic Billiard

1.3.1 Results not turning corners

When the particle doesn't go around a corner, Figure 1.1b, there are only four possible values for the slope of the trajectory inside Ω, we take advantage of this similarity with classical billiards and use it to unfold the trajectory 3.1.

In chapter 3 we introduce and prove some results involving Sturmian sequences of the unfolded inverse magnetic billiard trajectory.
Section 3.2 presents the case when the particle does not turn a corner and the initial velocity has rational slope.
The case when the initial velocity takes any given value was presented in section 3.3.
The two main results in this part are given by:

- Theorem 1: gives a partial classification of periodic orbits that don't turn corners. We give sufficient conditions for certain values of rational slopes, in order to get a periodic orbit.

- Theorem 2: gives existence of periodic orbits for any given initial velocity. This is the most surprising result that separates the inverse magnetic billiard from the classical case: we have periodic orbits for irrational slopes, see Figure 3.12.

At the end of this chapter, we have the most general classification of orbits 10, where we establish that the only orbits that don't turn corners are periodic.

1.3.2 Results turning corners

When an orbit turns a corning, in general, we can't control the values of the velocities. For the generic case, we could obtain a dense orbit in both variables: s, and θ (point on $\partial\Omega$ and angle with respect $\partial\Omega$). See for example Figure 4.3b
For this reason, we use numerical methods in chapter 4 to give evidence of several observed behaviors:

- Section 4.1 presents the Poincaré sections of the phase space for different conditions, showing the mixing or chaotic behavior depending on the strength of the magnetic field.

- Section 4.2 gives the Lyapunov exponent for the billiard 1.1.2 as a function of the magnetic field B. This is the stronger numerical evidence about how chaotic is the system. We found a jump discontinuity when $B \to \infty$. The biggest surprise was when $B \to 0$, we found that the system has Lyapunov exponent practically 0.

- Given the surprise described in the last item, we provide a conjecture about the existence of caustics when B is small enough.

Chapter 2

The Billiard Map

2.1 Description of dynamics on the square

Consider the dynamical system 1.1.2, the magnetic field 1.1.1, and take Ω as the unit square:

$$\Omega = \{q = (x, y) | 0 \leq x \leq 1, 0 \leq y \leq 1\}.$$

Initial conditions $q_0, \dot{q_0}$ for 1.1.2 can be associated with a pair

$$(s_0, \theta_0) \in (0, L) \times (0, \pi).$$

L is the length of $\partial\Omega$, s_0 represents a point on one edge of $\partial\Omega$ which we call the "entering edge", and θ_0 is the angle formed by $\dot{q_0}$ and $\partial\Omega$. For our case $L = 4$, see Figures 2.1, 2.2. Following the billiard's notation, these coordinates for initial conditions are called Birkhoff coordinates; even if our billiard is not smooth - a condition for "Birkhoff" billiards - we will use this denomination.

The particle moves inside Ω in straight line at angle θ_0 with respect to its side

until it hits the boundary again at $(s_1, \theta_1) \in (0, L) \times (0, \pi)$, the "exiting point" on some other edge, called the "exiting side" (Figure 2.2).

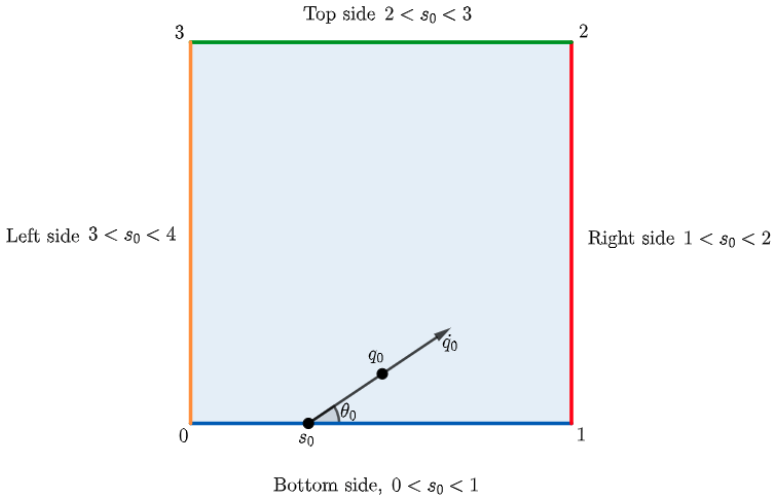

Figure 2.1: Initial conditions

After that, the particle moves exterior to Ω along an arc of a circle to be described and then re-enters Ω at the next entering side at the point and direction labeled (s_2, θ_2), the next "entering point".

The dynamical map that we are studying is the concatenation $(s_0, \theta_0) \mapsto (s_2, \theta_2)$. To figure out the arc of the circle outside Ω along which the particle travels, fix the particle's charge to be -1, its mass to be $m = 1$, and its speed to be $|v| = |\dot{q}| = 1$; furthermore, take a positive magnitude of B for the magnetic field. Then, outside Ω, the particle travels counterclockwise along a circle whose Larmor radius is $r = \frac{1}{B}$ and which is tangent to the line joining s_0 to s_1, that is, to the interior part of the trajectory.

Which edge s_2 lies on, depends on the location of s_1 and B, since different radii of the exterior circle will lead to different re-entry sides at (s_2, θ_2). The intermediate map $(s_1, \theta_1) \to (s_2, \theta_2)$ will be referred to as the *magnetic bounce*.

As soon as it hits Ω again on re-entry, the particle moves in a straight line. The line is tangent to the circle of its previous trajectory at the point of entry (see figure 2.2).

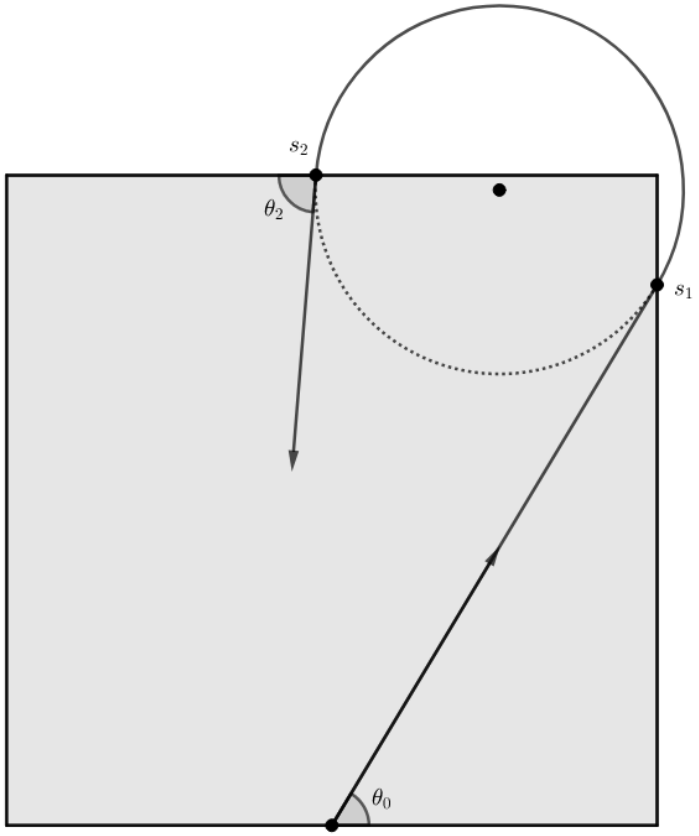

Figure 2.2: One bounce in the magnetic billiard: s_0 and s_2 are on entering edges,

The dynamics of 1.1.2, in this setting, can also be described by a map

$$F : \Sigma^2 \to \Sigma^2$$

$$F(s_0, \theta_0) = (s_2, \theta_2)$$

where $\Sigma^2 = \{(s, \theta) | 0 \leq s \leq 4, \quad 0 < \theta < \pi\} = \partial\Omega \times (0, \pi)$ is the space of

directed unit vectors toward the interior of Ω with initial points on the boundary. The map F can be decomposed as

$$F = F_1 \circ F_2 \tag{2.1.1}$$

where F_2 is the exterior magnetic bounce and F_1 is the "straight line" map $(s_0, \theta_0) \to (s_1, \theta_1)$.

We want to study the dynamics of this billiard-type map. One of the most challenging aspect of this investigation concerns trajectories that go around a corner, which are most of them. See figures 2.2 1.1a. The map is apparently chaotic, and all the chaos seems to come from turning around corners.

As we said before, it helps to not only consider the discrete map $(s_0, \theta_0) \to (s_2, \theta_2)$ but also the continuous trajectory $\gamma(t)$ which led to it. This curve $\gamma(t)$ is a C^1 - curve made of line segments inside Ω and circular arcs outside Ω and is the solution to the (discontinuous) ODE (1.1.2) with initial conditions $\gamma(0) \in \partial\Omega$, $\dot{\gamma}(0) = (\cos\theta_0, \sin\theta_0)$. We will also refer to $\gamma(t)$ as an orbit.

The main obstruction to carrying out our analysis to a complete picture of the dynamics proved to be complications arising from orbits going around corners (Fig 2.3).

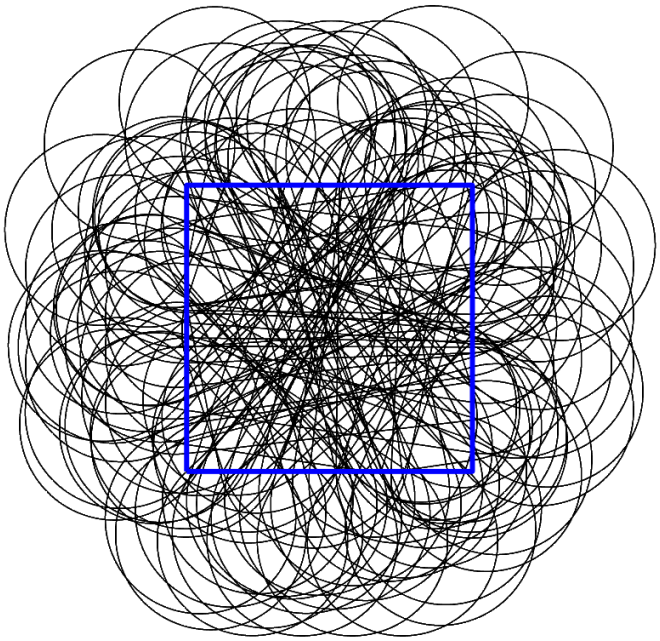

Figure 2.3: Going around corners

To underline this complication, we investigated a simple model of tables with only one or two corners. We were able to show that there exist orbits that turn the corner as many times as you like before continuing 'to another edge' along a straight line.

2.2 Extreme cases: $B \to 0, \infty$.

When the magnetic field tends to infinity, the time spent by the particle outside the billiard table decreases. In the limiting case $r = \lim_{B\to\infty} r_B = \lim_{B\to\infty} \frac{1}{B}$, the particle's motion is an elastic reflection from $\partial\Omega$, a typical bounce in the optic sense; this describes the dynamics of classic Birkhoff billiards, so the particle is trapped in the billiard table forever. See Figure 2.4 where $B = 10000$, although

pretty similar to the classic orbit, this orbit is different, notice how the space is filled in Figure 2.5, where the conditions are the same but we follow the orbit for more time.

When Ω is a square, the dynamics are well classified in terms of the slope ($\tan\theta$) of the initial velocity vector, getting a periodic orbit if rational and a dense one (on the billiard table) if irrational. However, the density of the orbits with irrational slope, in terms of our space $\Sigma^2 = (0, L) \times (0, \pi)$ is only on the first component (points on the boundary). This classical orbit has only four velocities/angles values. In our case, we can have a dense orbit in both components.

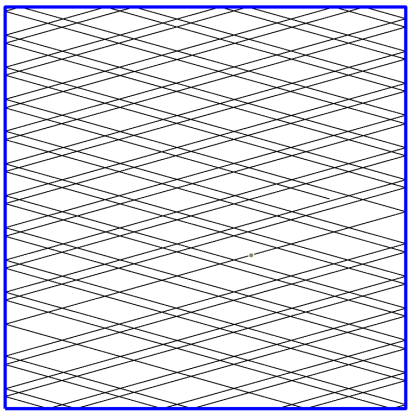

Figure 2.4

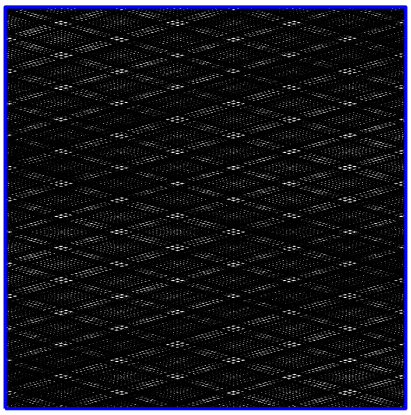

Figure 2.5

Note that in the Bunomovich billiard [Bun79], the classical case is completely chaotic, and the chaos measured by the Lyapunov exponent of the system directly correlates with the strength of the magnetic field. When Ω is a square, the classical case is completely integrable, but we will see 4.2 that chaos does not behave as smoothly as in the Bunimovich table.

On the other limit, the case when $r = \lim_{B \to 0} r_B$, the system becomes trivial, namely, the Larmor radius goes to infinity, so the particle returns to the billiard table after longer and longer periods. At the limit, the particle continues a straight trajectory all the time, so the only part of the trajectory inside the square is the initial segment. This orbit has only one exit and one entry point: the entry point is the same starting point, and the particle gets there again after infinite time, a completely integrable system. Figure 2.6 shows the case when $B = \frac{1}{10}$, and Figure 2.7 shows the first part of an orbit when $B = \frac{1}{1000}$.

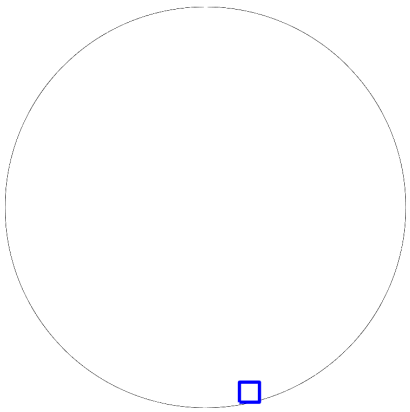

Figure 2.6: $B = \frac{1}{10}$

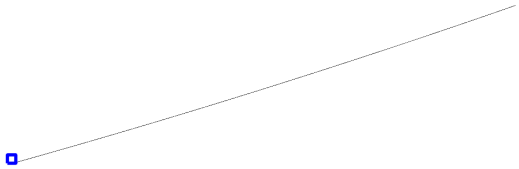

Figure 2.7: $B = \frac{1}{1000}$

2.3 Jacobian of the map

Using the traditional change of coordinates in Birkhoff billiards $u = -\cos\theta$, the map 2.1.1 F can be seen as $(s_0, u_0) \to (s_2, u_2)$, $F : (0, L) \times (-1, 1) \to (0, L) \times (-1, 1)$, a differentiable map of the open annulus. The Jacobian of its components $F_1(s_0, u_0) = (s_1, u_1)$ and $F_2(s_1, u_1) = (s_2, u_2)$ (see Figure 2.2), have the following

properties, which were computed by working out algebraic formulae for the F_i in terms of rational trigonometric functions (see [BK96] [Gas19]).

$$DF_1 = \begin{pmatrix} \frac{\partial s_1}{\partial s_0} & \frac{\partial s_1}{\partial u_0} \\ \frac{\partial u_1}{\partial s_0} & \frac{\partial u_1}{\partial u_0} \end{pmatrix} = \begin{pmatrix} \frac{-\sin\theta_0}{\sin\theta_1} & \frac{\partial s_1}{\partial u_0} \\ 0 & \frac{-\sin\theta_1}{\sin\theta_0} \end{pmatrix} \tag{2.3.1}$$

$$DF_2 = \begin{pmatrix} \frac{\partial s_2}{\partial s_1} & \frac{\partial s_2}{\partial u_1} \\ \frac{\partial u_2}{\partial s_1} & \frac{\partial u_2}{\partial u_1} \end{pmatrix} = \begin{pmatrix} \frac{-\sin(\vartheta-\theta_1)}{\sin\theta_2} & \frac{\partial s_1}{\partial u_0} \\ 0 & \frac{-\sin(\vartheta-\theta_2)}{\sin\theta_1} \end{pmatrix} \tag{2.3.2}$$

Here ϑ is twice the angle between the segment s_1s_2 and the tangent to the Larmor circle at s_1. This implies that $\det(DF_1) = \det(DF_2) = \det(DF) = 1$. Or that our map is area preserving.

2.4 Symmetries

Suppose for a moment that our unit square Ω is centered at the origin of $\mathbb{R}^2$, from Ω we inherit its symmetries, four rotations $(0, \frac{\pi}{2}, \pi, \frac{3\pi}{2})$ and four reflections (x-axis, y-axis and two diagonals). This group of symmetries is known as D_4, the Dihedral Group of order 4. This group is generated by the two elements $\mathbb{J}$ (rotation by $\pi/2$) and $R = \begin{pmatrix} -1 & 0 \\ 0 & 1 \end{pmatrix}$ (reflection about the y-axis). Here we prove some properties of the orbits using the symmetries of our billiard table and our dynamical system. We will use these to give a partial classification of periodic orbits.

Lemma 1. *If $\gamma(t)$ is an inverse billiard orbit (solution to 1.1.2) on Ω, then $\mathbb{J}\gamma(t)$ and $R\gamma(-t)$ are also orbits.*

Proof. Take $\tilde{\gamma}(t) = R\gamma(-t)$, then

$$\dot{\tilde{\gamma}}(t) = -R\dot{\gamma}(-t)$$

$$\ddot{\tilde{\gamma}}(t) = R\ddot{\gamma}(-t) = RB(\gamma)\mathbb{J}\dot{\gamma}(-t)$$

Since $R\mathbb{J} = -\mathbb{J}R$ we get

$$\ddot{\tilde{\gamma}}(t) = -B(\gamma)\mathbb{J}R\dot{\gamma}(-t) = B(\gamma)\mathbb{J}\dot{\tilde{\gamma}}(t)$$

This proves that $\tilde{\gamma}(t)$ is solution of (1.1.2). For $\hat{\gamma}(t) = \mathbb{J}\gamma(t)$ we get:

$$\dot{\hat{\gamma}}(t) = \mathbb{J}\dot{\gamma}(t)$$

$$\ddot{\hat{\gamma}}(t) = \mathbb{J}\ddot{\gamma}(t) = \mathbb{J}B(\gamma)\mathbb{J}\dot{\gamma}(t) = B(\gamma)\mathbb{J}\dot{\hat{\gamma}}(t)$$

□

Note that the previous lemma proves that a rotation of an orbit is an orbit, but not always the reflection is. So if $\gamma(t)$ is an orbit, $R(\gamma(t))$, in general, is not. The main reason for this is that orientation is reversed (R reverses it). Given a fixed B and point (s, θ), the dynamical system 1.1.2 has two orbits that could lead to the curve passing through s with slope $\tan\theta$ if we do not consider the orientation, see Figure 2.8.

Lemma 2. *If γ is a solution of (1.1.2), and one of the Larmor circles has it's center on one of the axis of symmetry of the square, with the corresponding intersection points on the same edge of the square, then γ is symmetric with respect to the same axis.*

More over if there are $n, k \in \mathbb{Z}$ and $T \in D_4$ such that $T(s_k, \theta_k) = (s_n, \theta_n)$ then

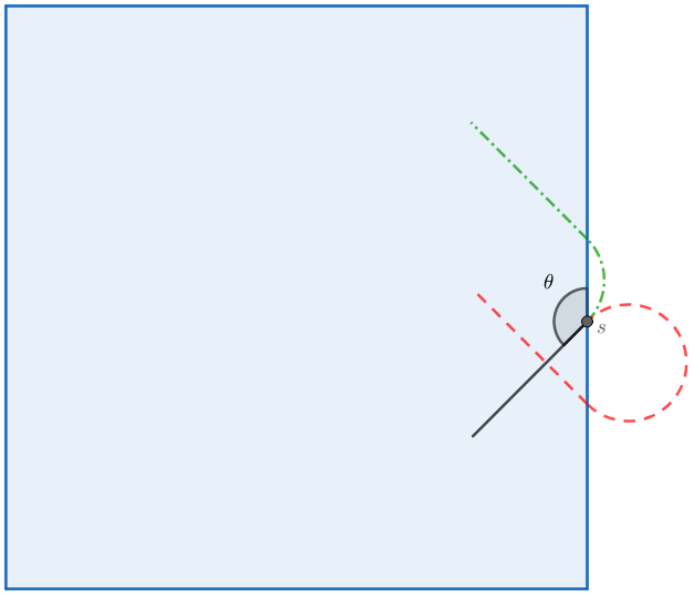

Figure 2.8: Two options for non oriented curves.

$T\gamma = \gamma$. *See Figure 2.9*

Proof. Every $T \in D_4$ is generated by $\mathbb{J}$ and R, since we have symmetry with one of the symmetry axis, the effect of R changing orientation if voided. This is, given B, s_0, θ_0, we have only one option for an orbit in Figure 2.8. □

Lemma 3. *For every initial conditions in Σ^2, for $R, R^2, \mathbb{J}R, \mathbb{J}R^2 \in D_4$ there is a magnetic field strength such that the solution satisfies (1.1.2) and $T\gamma = \gamma$*

Proof. Let $(s_0, \theta_0) \in (0,1) \times (0,\pi)$, take $B = \frac{\sin\theta_0}{|s_0 - 0.5|}$, the center of the Larmor circle for the first iteration of the map, lies on the vertical axis. The center of the Larmor circle lies on the one of the axis for R (vertical axis), $R\mathbb{J}^2$ (horizontal axis), $R\mathbb{J}$ or $\mathbb{J}R$ (two diagonals). □

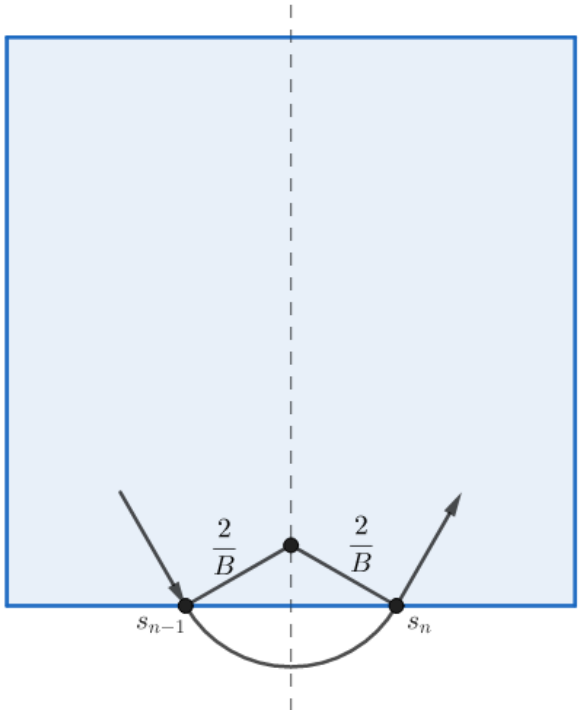

Figure 2.9: A portion of the trajectory if Larmor center is on a symmetry axis.

Chapter 3

No turning corners

In this chapter we concentrate on orbits that don't turn corners, this means that the magnetic portion of the orbit does not go around a corner on the outside of the billiard table Ω, see Figures 1.1b 3.1. In this case, the slope of the trajectory inside Ω can only take 4 possible values, the same ones it would take in the classical case $B = \infty$.

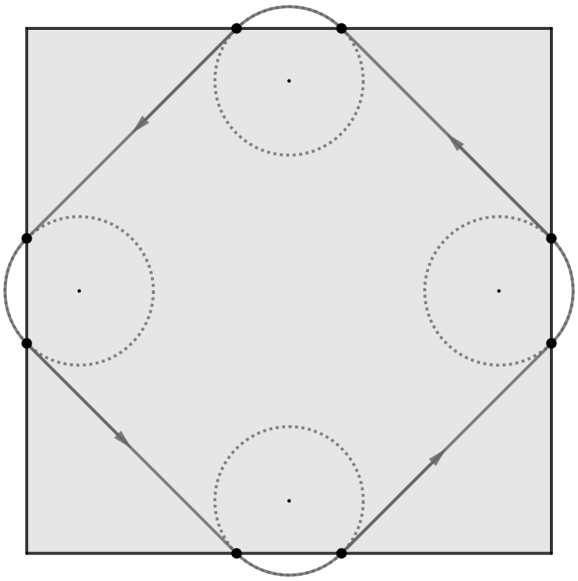

Figure 3.1: Example of no turning corners

Thanks to the symmetries on a square billiard table, we can assume our initial condition (s_0, θ_0) on the bottom side of the unit square $(0 < s_0 < 1)$. We will look for the returning map F (see 2.1) depending on the exiting side: right, top, or left side. The trajectory outside Ω not going around a corner, is equivalent to $\lfloor s_{n+1} \rfloor = \lfloor s_{n+2} \rfloor$, this means that the next entry point (s_{n+2}, θ_{n+2}) is on the same side as the exit point (s_{n+1}, θ_{n+1}).

Figure 3.1 shows an example of this case, $\theta = \frac{\pi}{4}$ or initial slope equal to 1, and radius small enough (depending on our initial conditions), such that the magnetic bounce $F_2(s_{n+1}, \theta_{n+1}) = (s_{n+2}, \theta_{n+2})$ happens on the same side of the square. Figures 3.2 3.3 3.4 show the three possible cases in this setting. Equations 3.0.1 3.0.2 3.0.3, show the values of the billiard map for their respective instance.

Bouncing on the right side of the square

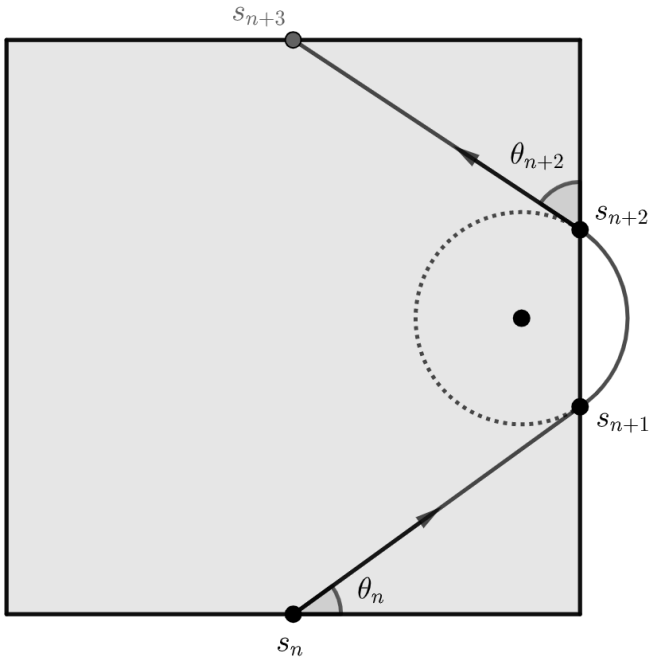

Figure 3.2: Bouncing on the right side

$$s_{n+1} = 1 + (1 - s_n)\tan\theta, \qquad s_{n+2} = s_{n+1} + \frac{2}{B}\cos\theta, \qquad \theta_{n+2} = \frac{\pi}{2} - \theta_n. \quad (3.0.1)$$

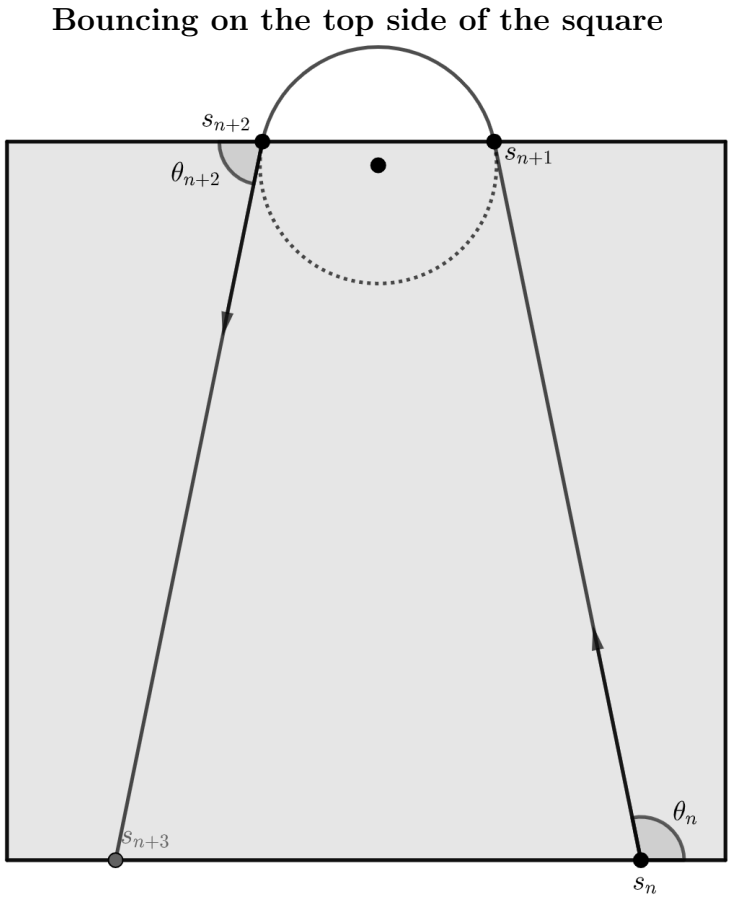

Figure 3.3: Bouncing on the top side

$$s_{n+1} = 3 - s_n - \cot\theta, \quad s_{n+2} = s_{n+1} + \frac{2}{B}\sin\theta, \quad \theta_{n+2} = \pi - \theta_n. \tag{3.0.2}$$

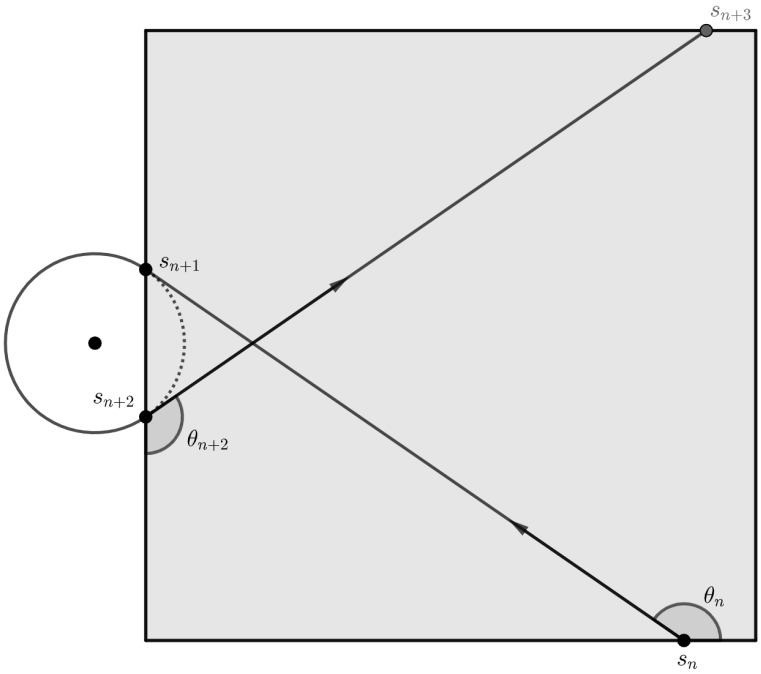

Figure 3.4: Bouncing on the left side

$$s_{n+1} = 4 + s_n \tan\theta, \quad s_{n+2} = s_{n+1} + \frac{2}{B}\cos\theta, \quad \theta_{n+2} = \frac{3\pi}{2} - \theta_n. \tag{3.0.3}$$

3.1 Symbolic Dynamics

Unfolding trajectories is a common method for analyzing polygonal billiards. (See [MT02], [Tab95].) Recall in classical square billiards, we can read off the full dynamics by drawing an arbitrary straight line $y = mx + b$ in the Cartesian plane and marking where this line intersects the "grid" of horizontal and vertical lattice lines obtained by setting either x or y to integers. See Figure 3.5. These intersection points have the form (m, y_j) or (x_j, n), $m, n \in \mathbb{Z}$. To obtain $(s_j, \theta_j) \in T_-\partial\Omega = \Sigma^2$ from these crossings, take s_j mod 1 to equal y_j or x_j mod 1 and record the angle that the line makes with the corresponding lattice edge. See figure 3.5.

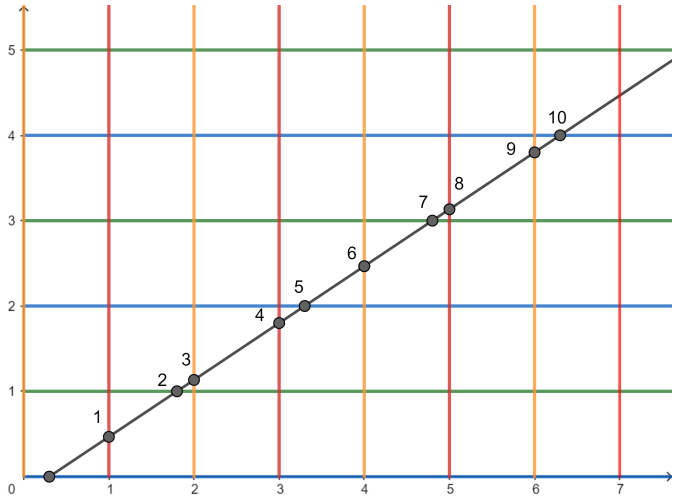

Figure 3.5: Case of slope $m = \frac{p}{q} = \frac{2}{3}$

In geometric terms, we are 'folding' the line $y = mx + b$ back up to fit in the square. In particular, only four values of θ_j are possible for any trajectory, since the slope of the line is constant.

We now recall more formally the process.

3.1.1 Sturmian sequences for classical square billiards

We begin by recalling notation and facts around classical square billiards and, in particular, the notion of the Sturmian sequence of a trajectory.

For the orbit given by the line $y = m(x - s_0)$, every point in orbit (s_j, θ_j) comes from a point $(x_j, mx_j + b)$ with $x_j \in \mathbb{Z}$ or $m(x_j - s_0) \in \mathbb{Z}$, we can record a V for the first case and a H for the second case. 'V' is for vertical line: the lines $x = n$ for $n \in \mathbb{Z}$ are vertical lines. Similarly 'H' is for horizontal line. The points mark where the line $y = m(x - s_0)$ crosses the lattice lines in our 'graph paper'. This yields to the 'Sturmian Sequence' of the orbit, a sequence of V's and H's that depend on s_0

$$...V^{n_0}H^{n_1}V^{n_2}H^{n_3}V^{n_4}H^{n_5}..., \text{ where } n_j \in \{0,1\} \tag{3.1.1}$$

Example 3.1.1. For figure 3.5 the Sturmian Word is

$$VHVVHVHVVH = V^1H^1V^1H^0V^1H^1V^1H^1V^1H^0V^1H^1$$

so $n_4 = n_{10} = 0$ and $n_j = 1$ for $j \neq 4, 10$.

Another possibility, for a different intercept but the same slope (say for the line $y = 1/3(x - 0.9)$) is

$$VVHVHVVHVH$$

Note that when viewed as periodic words (e.g., written on a circle), they are the same word: take the first VH of the first word and place it at the end of the word to form the second word.

It is important to remark that this sequence is defined if the orbit does not hit any lattice points (see [MH40], [DM15]). To get the Sturmian sequence, we could get around it by shifting the line and avoiding the corners - getting a different orbit in our dynamical system, and this is why we request our orbit not to hit corners.

Lemma 4. *If m is rational, the Sturmian sequence does not depend on the choice of the intercept.*

This lemma lets us talk about the 'Sturmian Word' for periodic orbits ($m \in \mathbb{Q}$ for classical billiards).

Lemma 5. *The Sturmian Sequence is periodic if and only if the trajectory is periodic.*

When the trajectory is not periodic ($m \notin \mathbb{Q}$), the Sturmian Sequence has a non-trivial dependency on s_0, and we can not say much about it.

Let σ_ℓ be the reflection in the plane about the line ℓ, and let

$$S(\Omega) = \{\sigma_{l_1}, \sigma_{l_2}, \sigma_{l_3}, \sigma_{l_4}\}$$

be the four reflections about the four lines making up the boundary of our square Ω. Let $A(\Omega)$ be the group of motions of the plane generated by $S(\Omega)$ [MT02]. Every copy of Ω involved in the unfolding is the image of Ω under an element of $A(\Omega)$. Each generator $\sigma \in S(\Omega)$ reverses the orientation of the orbit. The composition of an even number of generators will preserve orientation.

Since we also want to keep track of directions/velocities (our θ or slopes m can be represented by elements on $\mathbb{S}^1$), we take $G(\Omega)$ the subgroup of the orthogonal group generated by reflections through the vertical and horizontal axis. When a billiard orbit bounces on a side l_i of Ω, the direction $\theta \in \mathbb{S}^1$ is changed by the action of the element of $G(\Omega)$, which is the projection of σ_{l_i} to $G(\Omega)$. In our unit square case, the possible directions of the orbits are just four - like we mentioned before.

The obtained sequence of reflections $\{\sigma_k\}_{k\in\mathbb{Z}} \subset A(\Omega)$ in the unfolding can be related to the sequence $\{(-1)^k\}$ and paired with the previous Sturmian Sequence, to create an oriented version of the Sturmian Sequence:

$$\left\{(-1)^k V^{n_{2k}} H^{n_{2k+1}}\right\}_{k\in\mathbb{Z}} \tag{3.1.2}$$

If the orbit is periodic, to the Sturmian Word of finite length L, we can calculate

$$S = \sum_{k=0}^{L/2} (-1)^k V^{n_{2k}} H^{n_{2k+1}} \tag{3.1.3}$$

This sum will result in an expression of the form $aH + bV$, $a, b \in \mathbb{Z}$ and does not depend on the intercept if the orbit is periodic.

Example 3.1.2. In figure 3.5 for $p/q = 2/3$,

$$S = V - H + V - V + H - V + H - V + V - H = 0.$$

3.1.2 Sturmian sequences for inverse magnetic billiards

Let us now explore how much of the classical theory carries over to our magnetic billiards.

In magnetic billiards, folding and unfolding are less valuable due to turning corners, but they help us understand periodic orbits in certain situations. Without turning corners, we can use the same process for classical billiards; at every bounce, the group $A(\Omega)$ acts and changes the orientation from the previous bounce. The direction will coincide with the direction of the classical billiard. The shift of the orbit at every magnetic bounce makes the intercept with the lattice $\mathbb{Z} \times \mathbb{Z}$ different. After unfolding, between every two points $F^k(s_0, \theta_0) = (s_{2k}, \theta_{2k})$ and $F^{k+1}(s_0, \theta_0)$ the unfolded orbit has the orientation preserved if k is even.

We will now use the term "lattice edge" for any edge, vertical or horizontal, of length one that joins two lattice points. If we ask for not turning corners, then the entering and exiting sides are the same: (s_{2n}, θ_{2n}) and $(s_{2n-1}, \theta_{2n-1})$ lie the same lattice edge and moreover $\theta_{2n} = \sigma_{l_i} \theta_{2(n+1)}$ for some i. Since the directions (corresponding to θ_n) will be on the same $G(\Omega)$-orbit, the inverse magnetic orbit will have its segments (corresponding to the orbit inside the billiard table Ω) on the parallel lines with equations:

$$y = m(x - s_0 + a\hat{H}) + b\hat{V}. \tag{3.1.4}$$

where $a, b \in \mathbb{Z}$ and

$$\hat{H} = \frac{2}{B}\sin\theta_0 = \frac{2m}{B\sqrt{m^2+1}} \qquad \hat{V} = \frac{2}{B}\cos\theta_0 = \frac{2}{B\sqrt{m^2+1}} \tag{3.1.5}$$

$\hat{H}$ and $\hat{V}$ correspond to the shifts from the magnetic bounce on the same side of Ω covered in the equations 3.0.2 3.0.1 3.0.3, see Figure 3.6. Compare to the classical case, when the orbit corresponds to the single line $y = m(x - s_0)$.

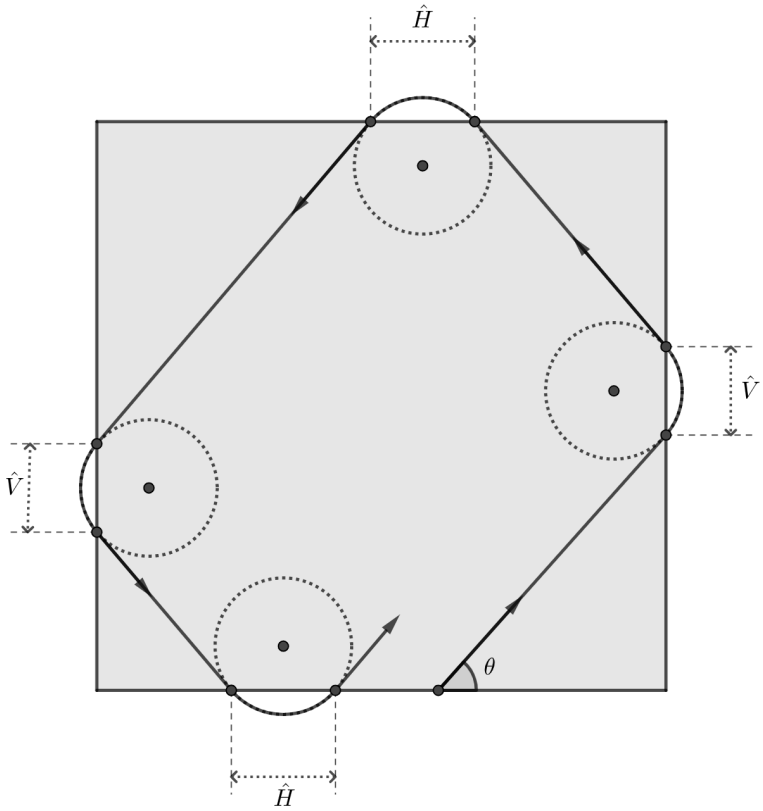

Figure 3.6: Vertical and horizontal shifts

For this unfolded orbit, we can define the same ordered Sturmian sequence

3.1.2. In the presence of a magnetic field, this has a better application, each appearance of a positive (negative) V means a shift of $\hat{V}$ units upwards (downwards) of the orbit, the same for each appearance of H or $-H$ will mean a shift to the right or the left by $\hat{H}$ units.

We can define the same sum 3.1.3, and if $S = 0$, this means we had the same vertical displacements that preserved the orientation as ones that did not, the same for the horizontal displacements.

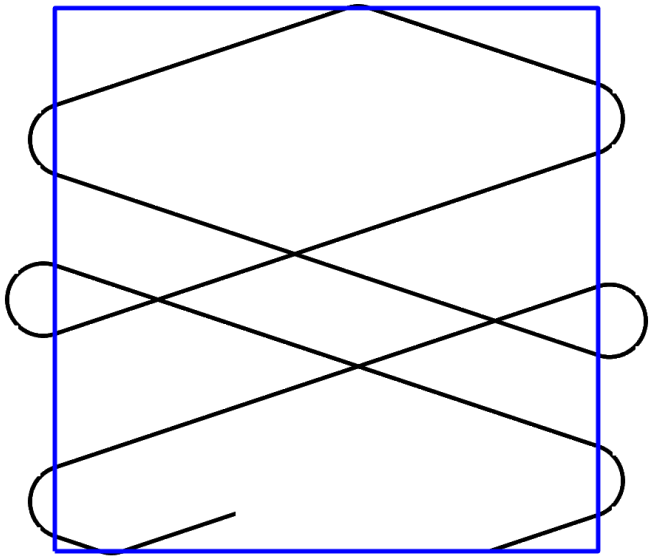

Figure 3.7: $B = 15$, Slope $1/3$, $s_0 = 0.8$

Example 3.1.3. Take $p/q = 1/3$, the figure 3.7 shows the case when $s_0 = 0.8$ and $B = 15$, something similar will happen for all $s_0 \in (0, 1)$ that don't hit or turn corners. The unfolded orbit after eight iterations of the billiard map is shown in 3.8, in these conditions we have

$$S = V - V + V - H + V - V + V - H = 2V - 2H \neq 0.$$

We can see the shift on the bottom side of Figure 3.7, where the two en-

trance points are separated by a considerable distance, compared to the classical case when they coincide. In Figure 3.8, the original inverse magnetic orbit is represented in green (web version), the classical trajectory is the dotted gray line. Every piece of the unfolded inverse magnetic orbit is represented with a black solid or dashed line. A dashed line represents an inversion of the orientation, a solid one represents orientation preserved.

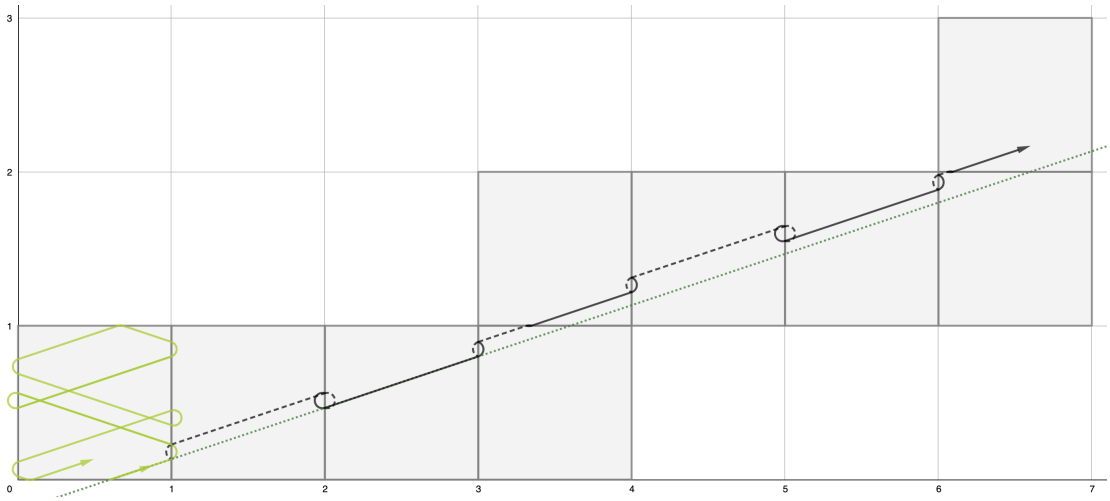

Figure 3.8: Unfolded $B = 15$, $\tan\theta = \frac{1}{3}$

The values a and b in 3.1.4 are the coefficients of V and H in the partial sums of 3.1.3. To study when the orbit is periodic, we want $s_{2n} = s_0$ for some n, this will happen on one of the lines $y = 2k$, $k \in \mathbb{Z}$. The orbit points on these lines are given by $(x^*, 2k)$ where

$$x^* = \frac{2k}{m} - \frac{b\hat{V}}{m} - a\hat{H} + s_0$$

In order to coincide with the original piece of orbit, we need $x - s_0 \in \mathbb{Z}$, or equivalently:

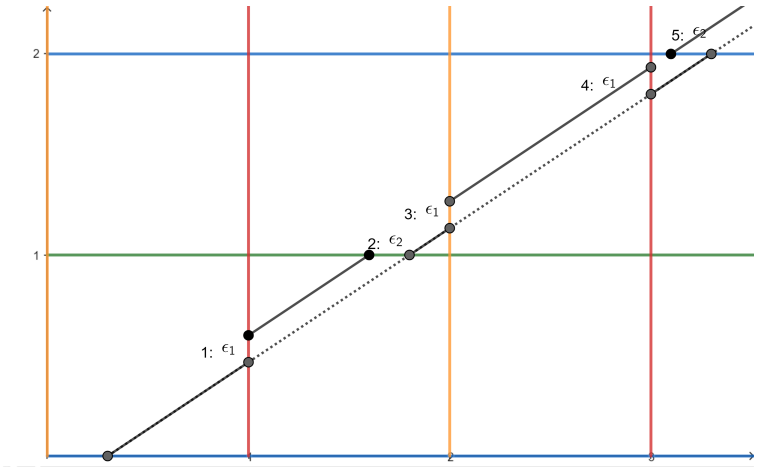

Figure 3.9: Case of rational slope $\frac{p}{q}$

$$\frac{2k}{m} - \frac{b\hat{V}}{m} - a\hat{H} \in \mathbb{Z} \tag{3.1.6}$$

Equation 3.1.6 is a **sufficient condition** for our orbit to close.

3.2 Rational slope ($\tan\boldsymbol{\theta} \in \mathbb{Q}$)

When the slope of the orbit ($\tan(\theta)$) is a rational number $\frac{p}{q}$ with p and q relatively prime, for classical billiards, the orbit is periodic. We would like to say that the corresponding orbits are periodic for our inverse magnetic billiards, but this is not always true. For example, see Figures 2.3 and 3.7. This section investigates when rational slopes lead to periodic magnetic orbits.

The figure 3.9 shows the first bounces for the example $p/q = 2/3$. Every shift has another one that cancels it out. After $2(p+q)$ bounces, we are at the initial conditions again. The complete picture is shown in Figure 3.10.

One special case is when the unfolded trajectory crosses the same sides as

the unfolded classical one. Since the slope is $\frac{p}{q}$ we will have $2(p+q)$ bounces. In the inverse magnetic case, these bounces are when the particle exits and returns from and to the billiard table. The figure 3.5 shows the case of slope $2/3$, where we have $2(2+3) = 10$ bounces in the classical billiard.

Lemma 6. *If the orbit doesn't turn corners,* $\tan\theta \in \mathbb{Q}$*, and* $2/B < \min\{|s_0 - k/q|, |s_0 p/q - k/p| : k \in \mathbb{Z}\}$*, then the Sturmian sequence (3.1.2) doesn't depend on* s_0*.*

Proof. Notice that the requirement of not turning corners plus having a small radius is equivalent to having the same Sturmian sequence as the classic billiards linear orbit. Take $\tan\theta = \frac{p}{q}$, p and q relatively prime. The Sturmian sequence will change between two initial conditions that lead us to hit corners. The initial conditions that do this are the multiples of $1/q$. Between any two of these numbers $(k/q < s_0 < (k+1)/q)$, the sequence is constant since we always start on a horizontal line, and p and q are relatively prime, the orbit will not hit lattice points in the $2q \times 2p$ area of the plane.
If $s_0 \in (0,1)$ is on another interval of length $1/q$ the sequence consists of the same finite parts (words). (see [DM15]) □

Lemma 7. *If* $p + q = 2k + 1$ *for some* $k \in \mathbb{Z}$ *then* $S = 0$*.*

Proof. Assuming we do not turn corners and $\tan\theta = \frac{p}{q}$, the Sturmian sequence will have a finite portion (Sturmian word) that repeats itself infinitely. In the area, $2p \times 2q$, this word repeats itself twice. The first appearance of the word is the one given in the area $p \times q$, where the trajectory hits $p + q$ lines of the grid $\mathbb{Z} \times \mathbb{Z}$. If $p + q = 2k + 1$ then $(-1)^{2k+1} = -1$, this means the second appearance of the word will have opposite signs of the first one. □

Using the general computation done before in (3.1.6) with $m = p/q$, after $2(p+q)$ magnetic bounces we will end up on the same edge as s_0, since we are not turning corners. In the unfolded lattice, this corresponds to the line $y = 2p$. The two lines, classic and inverse magnetic, will differ by

$$a\hat{H} + \frac{p}{q}b\hat{V} \tag{3.2.1}$$

the lemma 7 gives us that this quantity is zero for $p+q$ odd. In all the cases, this means that the shift after $2(p+q)$ bounces will be

$$a\frac{2}{B}\frac{p}{\sqrt{p^2+q^2}} + b\frac{p}{q}\frac{2}{B}\frac{q}{\sqrt{p^2+q^2}} = \frac{2}{pB\sqrt{p^2+q^2}}\left(ap^2+bq^2\right) \tag{3.2.2}$$

What we want in order to have a periodic orbit is

$$\frac{2}{pB\sqrt{p^2+q^2}}\left(ap^2+bq^2\right) = K, \qquad K \in \mathbb{Z} \tag{3.2.3}$$

The unfolded lattice for the magnetic billiard with these conditions (a radius small enough to not turn corners) is as shown in Figure 3.10.

Theorem 1. *Take initial conditions (s_0, θ_0). If $\tan\theta_0 = \frac{p}{q} \in \mathbb{Q}$, $p+q \in 2\mathbb{Z}+1$, p, q relatively primes, $s_0 \notin \mathbb{Z}/p\mathbb{Z}$ and $2/B < \min\{|s_0 - k/q|, |s_0 p/q - k/p| : k \in \mathbb{Z}\}$, then the orbit through (s_0, θ_0) is periodic. For fixed p/q, the set of s_0 satisfying these conditions form a non-empty open set.*

Proof. The condition $s_0 \neq \mathbb{Z}p$ deletes the cases where the orbit hits corners. We can take $B > 2/\min\{|s_0\frac{p}{q} - \frac{1}{q}|, |s_0 - \frac{1}{p}|\}$ so we actually ensure that the radius of the circle is small enough to stay in the same side of the square. Since $\frac{2}{B}$ is the diameter of the circle, with this condition, we are securing that the exiting point

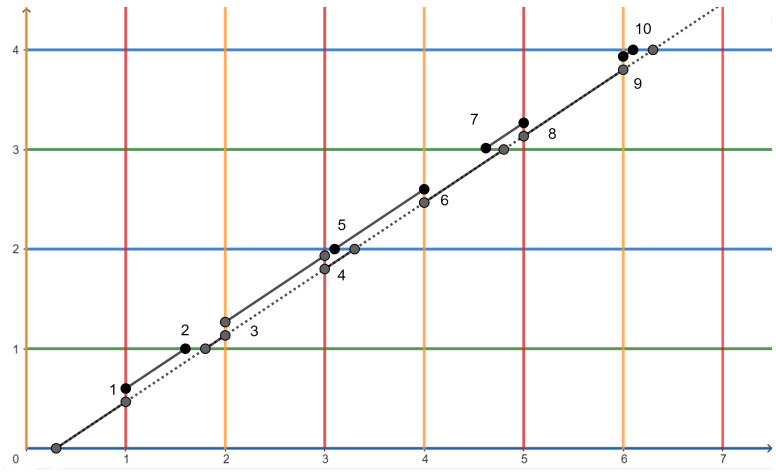

Figure 3.10: Case of slope $\frac{p}{q} = \frac{2}{3}$

(s_1, θ_1) is at least at one diameter distance from all the corners. This condition on B makes the diameter of the circle smaller than all the distances between the orbit and the points in the lattice $\mathbb{Z} \times \mathbb{Z}$.

The closest that a straight line that starts at the origin with slope $\frac{p}{q}$ gets to a point in the lattice is $\min\{|k/q|, |k/p| : k \in \mathbb{Z}\}$. A line that starts at $(s_0, 0)$ will get shifted at the intersection points (with the lattice lines) by s_0 to the right on the horizontal lines, and by $s_0\frac{p}{q}$ downwards in the vertical lines. This means that we can get as close as we want to the points in the lattice, depending on s_0. Once you fix s_0, the closest you get is $\min\{|s_0 - k/q|, |s_0 p/q - k/p| : k \in \mathbb{Z}\}$.

We will have $2(p+q)$ shifts of the classical trajectory in our setting. These shifts can be $\hat{V} = \frac{2}{B}\cos\theta_n$ or $\hat{H} = \frac{2}{B}\sin\theta_n$, depending on the side of the square where the magnetic bounce occurs: $\hat{V}$ for a vertical side (red or orange in the grid for the web version of this document), and $\hat{H}$ for horizontal sides (blue and green on the grid). These numbers correspond to the formulas in the previous section 3.1.5.

The unfolded trajectory in the plane will cross $2q$ vertical lattice lines and $2p$ horizontal lattice lines; p of those crossing correspond to the lower side of the square, p to the upper side, q to the left side, and q to the right side. In our notation, this means $2p$ shifts of $\hat{H}$ units horizontally and $2q$ shifts of $\hat{V}$ units vertically. Since the rotation is counter-clockwise, the shifting on the lower side is always to the right, upwards on the right side, to the left on the top side, and downwards on the left side. The shifting is towards opposite directions on parallel sides. Because $p+q$ is odd, we have that $S = 0$ (Lemma 7), so the orientations are preserved. With this, we have that the shifts will cancel each other. We will obtain $(s_0, \theta_0) = (s_{2(p+q)}, \theta_{2(p+q)})$, this proves the theorem.

□

We've proved the existence and partially classified periodic orbits that have rational slopes and do not turn corners. The classification is not complete, namely, we don't have conditions for a periodic orbit when the slope is p/q with $p+q$ even and which don't turn corners, but we do know is that if they exist, the period is not $2(p+q)$. To complete the classification, we should show that the equation 3.1.6 has solutions, but we don't know how a and b generally behave in the case $p+q$ even.

The classification is also incomplete because these are not the only periodic orbits. Depending on B we can have orbits with rational slope $\frac{p}{q}$ and period less than $2(p+q)$. See the example in the figure 3.11 where $\tan\theta_0 = \frac{9}{32}$ but the period of the orbit is 8, not 288. See also the examples showed in Figures 3.13 3.12.

Notice that the symbolic dynamics, and the result above, can be generalized to regular polygons that tessellate the plane: triangles and hexagons.

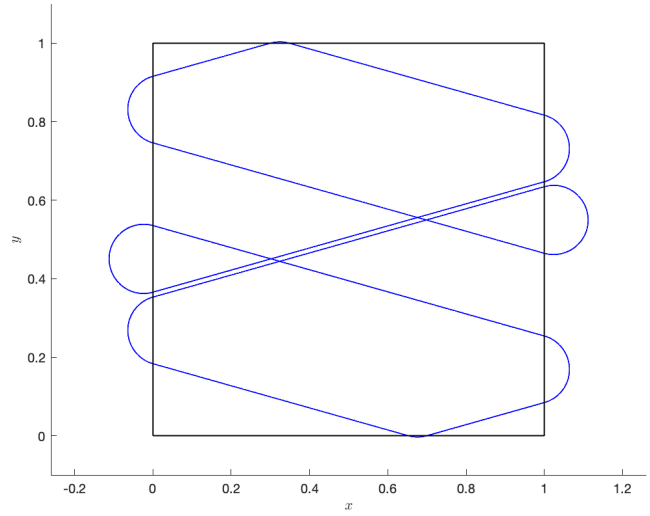

Figure 3.11: Slope $\frac{9}{32}$, $s_0 = 0.7$, period 8

3.3 General slopes

The symbolic dynamics we developed in chapter 3.1 are valid for any value of the slope. The previous chapter explored when the slope was rational, so we had a method to count or keep track of an orbit's unfolded trajectory while traveling through the lattice lines on our graph paper, ultimately leading to a control of the oriented Sturmian sequence 3.1.2 and the Sturmian sum 3.1.3.

When the slope is not rational, we do not have a method to keep track of the crossings. In classical billiards, the irrationally sloped line $y = mz + v$ represents a trajectory for an irrational flow on a torus. The entering points s_{2j}'s represent the orbit of the Poincare section of this flow. Thus, these s_{2j}'s for the classical problem are dense in the unit interval. We cannot use the same argument as

before and take the minimum distance to a lattice point over a finite area ($2p \times 2q$ rectangle in the rational case).

In a generic case, we would eventually have our magnetic particle close to a lattice point that it should turn a corner (see chapter 4). However, this is not always the case.

Theorem 2. *For every $\theta \in (0, \pi)$, there exist B and s_0 such that the solution to 1.1.2 is periodic.*

Proof. The equation 3.1.6 is valid for all $\theta \in (0, \pi)$.

We can rewrite the condition for periodicity as:

$$\frac{2k}{\tan\theta} - \frac{b}{\tan\theta}\frac{2}{B}\cos\theta - a\frac{2}{B}\sin\theta \in \mathbb{Z}$$

or

$$2k - b\frac{2}{B}\frac{1}{\sqrt{m^2+1}} - am\frac{2}{B}\frac{m}{\sqrt{m^2+1}} = Zm, \qquad Z \in \mathbb{Z}$$

If this equation has a solution, and we take a, b, k, Z as constants, we get a continuous function of B in terms of m:

$$B = \frac{2k\sqrt{m^2+1} - 2b - 2am^2}{Zm\sqrt{m^2+1}}. \tag{3.3.1}$$

m cannot be 0 since $\theta \in (0, \pi)$ - we don't allow initial velocities horizontal. Z cannot be 0, since it represents the horizontal distance traveled by the orbit - being 0 means that the orbit stayed the whole time at a single point.

When two orbits cross the same lattice lines and get to the same lattice edge when $y = 2k$, we will have a, b, k, Z constant.

For a big enough B, if we have a periodic orbit of slope $m = \tan\theta_0$, and starting point s_0, there is a neighborhood $U \subset (0, \pi)$ of θ_0 where the oriented Sturmian sequence 3.1.2 are the same, this implies that the Sturmian sum 3.1.3 is small enough, hence and a, b, k, Z do not change. Therefore, the equation 3.3.1 has a solution for every $\theta \in U$.

Theorem 1 finishes the proof since the slopes $m = p/q$, $p + q$ odd, are dense on $\mathbb{R}$. □

Theorem 2 gives us the existence of a periodic orbit for any value of the slope, irrational or rational, including the cases when the slope is p/q with $p + q$ even.

The same can be said about B. If there is a periodic orbit of 1.1.2 with initial conditions $\tan\theta$, s, and magnetic field B without turning corners, then there is a neighborhood $(B - e, B + e)$ where we can find solutions to our problem.

Note that the existence of periodic orbits for $B > 1$ is always secure, just taking the initial conditions $(1/B, \pi/2)$, but with this remark, we have something more substantial:

Lemma 8. *For any $B > 1$, there exist θ and an open set $(s - e, s + e) \subset (0, 1)$, such that the initial conditions $(s_0, theta)$, $s_0 \in (s-e, s+e)$ yields a periodic orbit for 1.1.2.*

Lemma 9. *For any $\theta \in (0, \pi)$, there exist a value of B and an open set $(s-e, s+e) \subset (0, 1)$, such that the initial conditions $(s_0, theta)$, $s_0 \in (s - e, s + e)$ yields a*

periodic orbit for 1.1.2.

Note that Theorem 1 and the previous results, secure the existence of infinite $2(k+1)$ periodic orbits for any $k \in \mathbb{N}$.

Example 3.3.1. As an illustration of the previous results, we show the cases when the slopes are $\frac{7}{24}, \frac{7}{25}, \frac{\pi}{11}$. All of them are close to each other. The picture in figure 3.12 show the three cases with the same initial starting point $s_0 = 0.5$ (different B), as theorem 2 says. The picture in figure 3.13 shows the same cases shifted to different initial points. We could translate any of the three orbits to an initial point in the interval $(0.3, 0.8)$. All the orbits we obtain here are periodic.

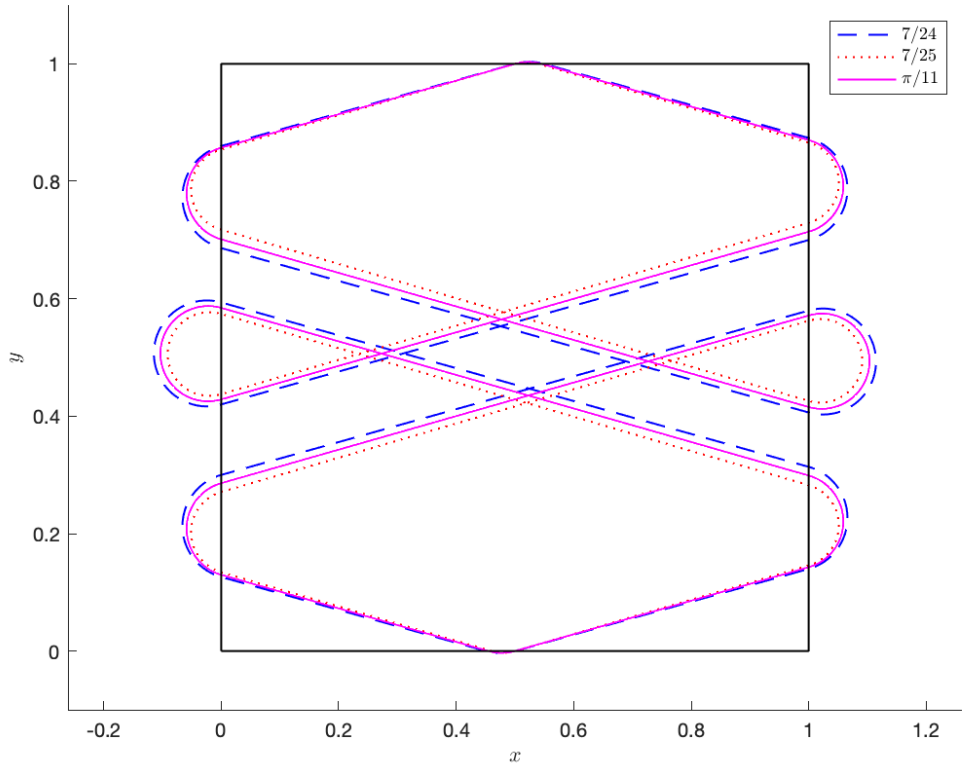

Figure 3.12: Slopes $\frac{7}{24}$, $\frac{7}{25}$, $\frac{\pi}{11}$, $s_0 = 0.5$, period 8

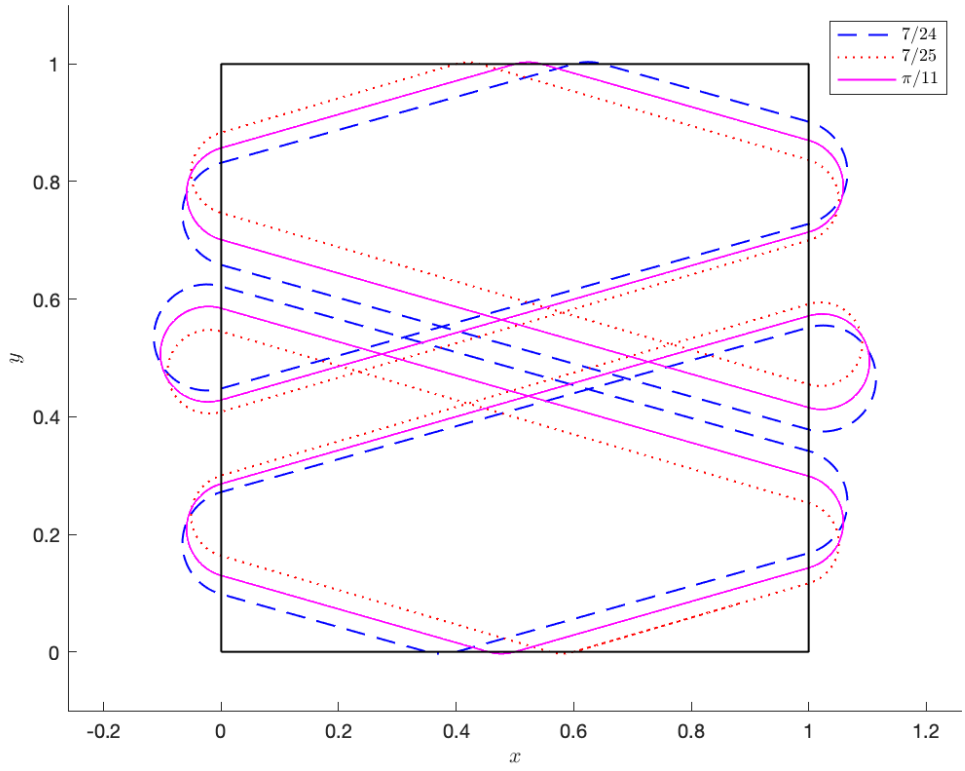

Figure 3.13: Slopes $\frac{7}{24}$, $\frac{7}{25}$, $\frac{\pi}{11}$, $s_0 = 0.3, 0.5, 0.7$, period 8

Lastly, we present a lemma that gives a full classification of these type of orbits that do not turn corners.

Lemma 10. *If an inverse magnetic billiard orbit 1.1.2 on the square doesn't turn a corner, it is periodic.*

Proof. If not periodic, one of the sides must fill out a dense set of points. This is because the lines 3.1.4 will be dense on a strip of the plane. Eventually one of the lines (corresponding to a segment of an orbit) will cross one lattice edge close enough to turn a corner, this is: there is a line 3.1.4 with distance less than $\frac{1}{B}$ to one of the lattice points $\mathbb{Z} \times \mathbb{Z}$. □

Chapter 4

Numerical evidence of chaos

In this chapter, we give numerical evidence that our billiard map tends to be chaotic.

After a turn of a corner the set of θ values is dense in most cases, the slope can be rational or irrational. Even though we can have periodic orbits that turn corners, see Figure 4.1. If the slope is rational, we are not necessarily in the conditions of Theorem 1, we have violated the condition of being away from a lattice point by the minimum established distance.

The Bunimovich stadium [Bun79] is a billiard table consisting of a square with two half circles attached at opposite sides, forming a smooth boundary, which is a well-known and studied problem. In the classical case, the case when $B \to \infty$, the Bunimovich billiard is ergodic and mixing, [VTCP03] proved that by the selection of B, we could control the chaos in this billiard system. In the same setting, when $B \to \infty$, square billiards are completely integrable, we were hoping to make a similar statement as [VTCP03] for our case.

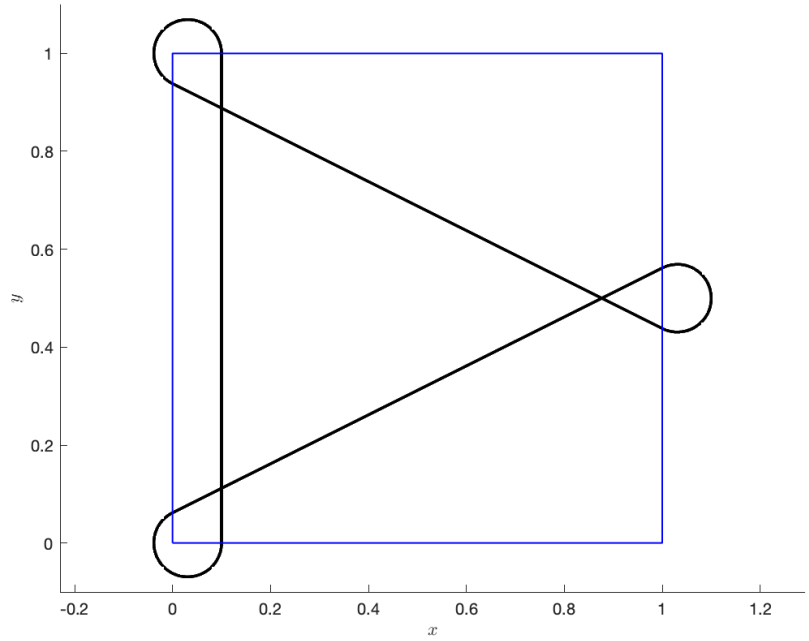

Figure 4.1: Periodic orbit turning corners.

Some words on the methods: for visualizing the solutions of 1.1.2 we use numerical integration of the ODE, and used the highest precision possible on the machine, reducing the numerical noise in the code.

To get the data points on Σ^2 for the map 2.1, the code was written in Python, providing exact numbers when possible - up to 10^{16} decimals.

Using this data, we calculated the Lyapunov exponent for the times the generated by 1.1.2 using the method described in [WSSV85]. We also followed the lead of [VTCP03] and used Jacobi fields to calculate the Lyapunov exponent and the phase space volume ratio.

4.1 Poincaré sections

Since we already studied the case when we were demanding the magnetic bounce to occur on the same side, we now turn to the case when the charged particle goes around at most one; this is the same as asking for

$$\lfloor s_1 \rfloor \mod 4 \quad = \quad \lfloor s_2 \rfloor + 1 \mod 4$$

where $F_2(s_1, u_1) = (s_2, u_2)$.

The system fulfills the last condition if $B < 1$, we limit the Larmor radius to be $r = \frac{1}{B} < 1$, and it will be small enough to go around at most one corner, so the entering side is the same or adjacent to the exiting side.

The figures show the Poincaré section of the phase space, $F^n(s_0, \theta_0) = (s_{2n}, \theta_{2n})$ for different numbers of iterations. We calculate the map $F : \Sigma^2 \to \Sigma^2$ with different initial conditions and radii. These are the points when the charged particle enters our billiard table, the magnetic-field free zone, and crosses the boundary $\partial\Omega$ at the point $s \in (0, L)$ with and angle θ with respect to $\partial\Omega$. Here we use the Birkhoff coordinates (s, u), $u = -\cos\theta$ in the depicted figures.

Example 4.1.1. We start with a small radius, $r = 0.02$. Taking a look at a periodic orbit, Figure 4.2a shows something similar to Figure 3.1, a periodic orbit of order 4, when initial velocity has slope 1.

With four different initial conditions, we get the different orbits in Figure 4.2b, depicted with different colors (web version). Some of them turn corners, so now we have more than one horizontal value.

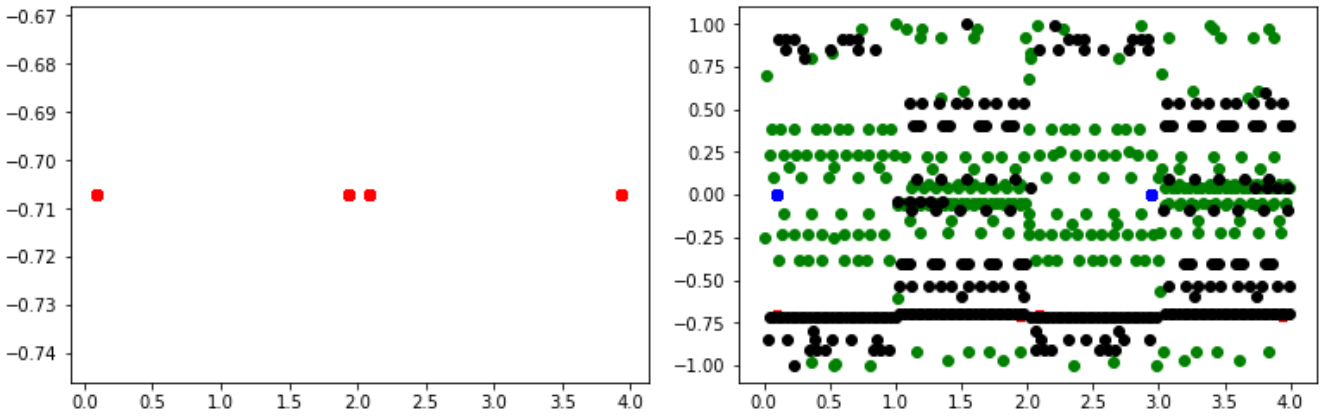

(a) A periodic orbit **(b)** Four orbits

Figure 4.2: Poincaré sections with $r = 0.02$

Figure 4.3a shows when we increase the number of iterations (1000), the phase space start to fill up. And when we go for 10000 bounces, we can observe in Figure 4.3b that all the phase space is virtually completely covered.

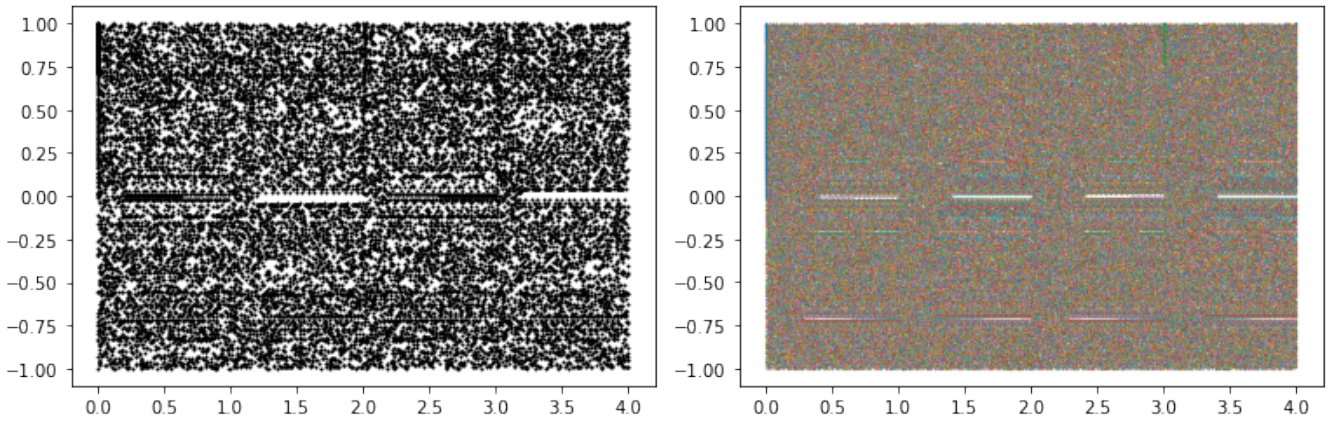

(a) 1300 bounces **(b)** 10000 bounces

Figure 4.3: More bounces with Poincaré sections with $r = 0.02$

Example 4.1.2. Trying with a bigger radius, $r = 0.49$ we encounter a piece-wise linear behavior.

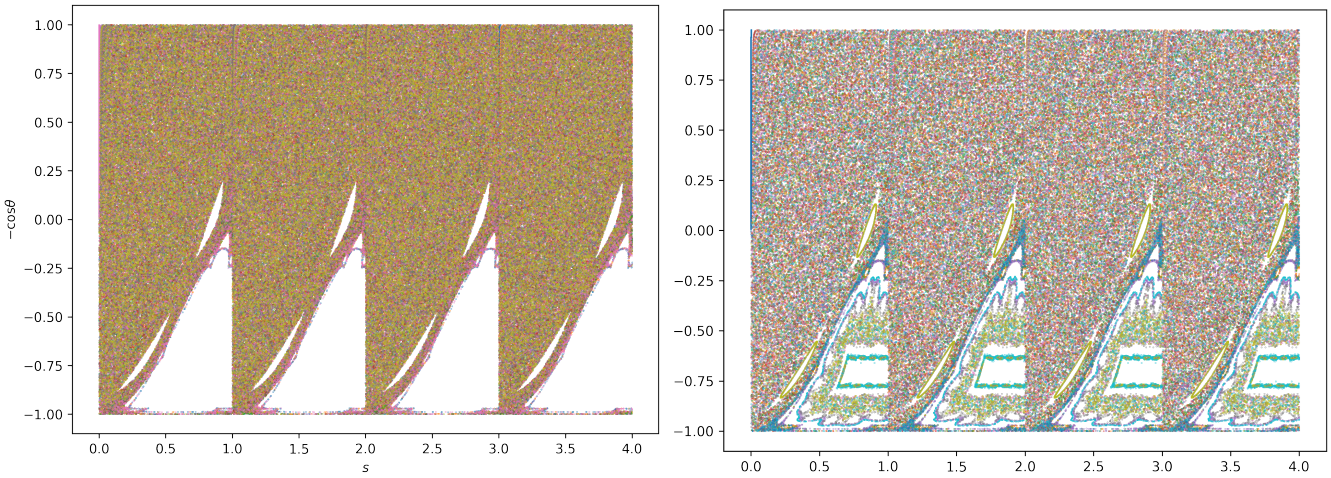

(a) Chaos only **(b)** Regular area filled

Figure 4.4: Poincaré sections with $r = 0.49$

Example 4.1.3. Figure 4.5 shows the case with $r = 0.85$, here is more clear that there is a piecewise linear behavior.

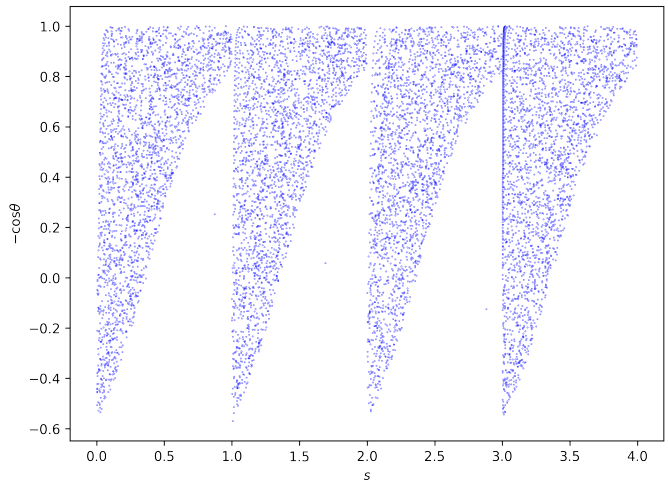

(a) One orbit

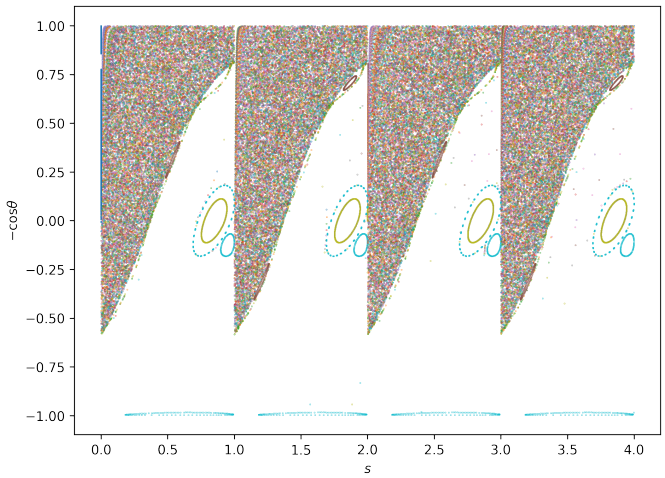

(b) 100 orbits

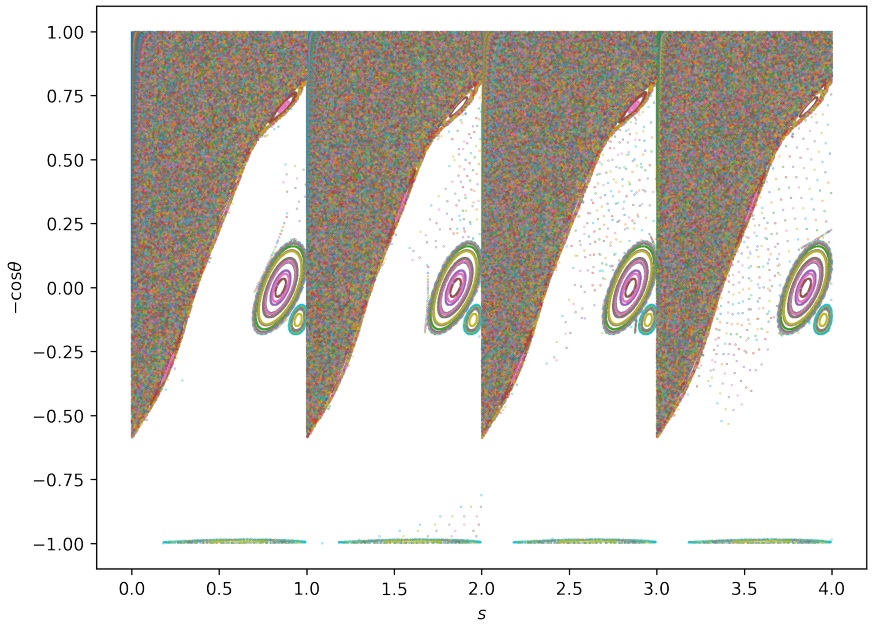

(c) 900 orbits

Figure 4.5: Poincaré sections with $r = 0.85$

Figure 4.5a, shows that we can fill the chaotic part with only one orbit. The regular regions are filled with different orbits coming from different initial conditions. Figures 4.5b and 4.5c show how we can fill the space when we go from 100 to 900 initial conditions. These initial conditions come from a uniformly

distributed grid on the phase space, the first case is a 10×10 grid, the latter is a 30×30, every color corresponds to one orbit (web version).

We can notice with the previous examples that as B increases, so does the chaotic parts of the Poincaré section. When B is large enough, the system is nearly completely chaotic. As B decreases, the Larmor radius increases and the regular regions of the phase space start to occupy more and more area.

To make these observations formal, we calculate the ratio of the regular area to the chaotic areas in the Poincaré section. We do this as a function of B or $r = \frac{1}{B}$, using the box counting method with a 1000×1000 grid of the square. As expected, this function is completely different for big and small values of B. When $B > 50$ the regular areas are almost negligible, and the system is nearly completely chaotic. However, when $r > 0.5$ the regular areas get bigger and occupy significant space of the phase space.

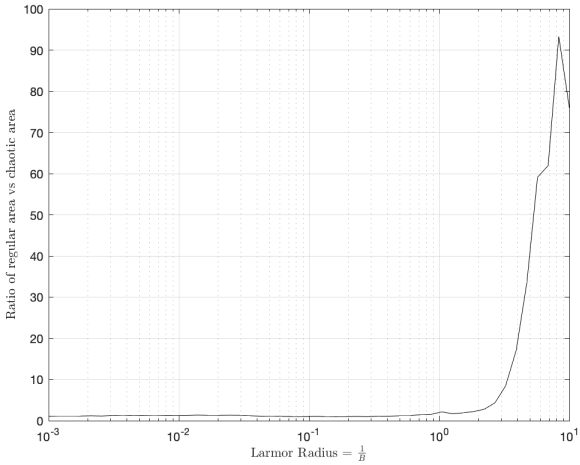

Figure 4.6: Ratio of regular area to chaotic area

4.2 Lyapunov exponent

There have been plenty of works on Billiards and chaos. Billiards is a playground for dynamical systems, in the 1980s [Woj85] [Woj86] showed cases that lead to non-vanishing Lyapunov exponents in a large class of billiards with convex pieces of the boundary.

Treating a solution orbit to 1.1.2 as a time series, we follow the algorithm described in [WSSV85] and [RCD93]. Nowadays, there are several methods to calculate the Lyapunov exponent of a time series, we found that most of them are pretty similar to this algorithm.

The algorithm selects an initial point $s_0 = \gamma(t_0)$ on a "fiducial" trajectory [WSSV85], finds it's closest neighbor, $n_0(t_0)$, and store the distance between them, $d_0 = ||\gamma(t_0) - n_0(t_0)||$. Follow the orbit of $n_0(t_0)$ until the separation is bigger than a tolerance $d_1' = ||\gamma(t_1) - n_0(t_1)|| > \epsilon$. Find the closest neighbor to $s_1 = \gamma(t_1)$, store $d_1 = ||\gamma(t_1) - n_1(t_1)||$, follow n_1's orbit until $d_2' = ||\gamma(t_2) - n_1(t_2)|| > \epsilon$. The biggest Lyapunov exponent is given by

$$\lambda = \frac{1}{t_N - t_0} \sum_{1}^{M} \log_2 \frac{d_i'}{d_{i-1}}$$

In the process, we use Grand-Schmidt on every step to normalize the frame $\{\dot{\gamma}, \dot{\gamma}^{\perp}\}$ to the "fiducial" trajectory.

We also used Jacobi fields to calculate the same Lyapunov exponent, getting similar results. This is the same method used in [VTCP03], and previously used in magnetic billiards on [Tas97]. For this method, we looked for the change of the Jacobi fields along a particular trajectory. We can define the Jacobi field as

$\frac{\partial \gamma_\epsilon(t)}{\partial \epsilon}|_{\epsilon=0}$, where γ_ϵ is a one-parameter family of orbits, γ_0 plays the role of the correspondent "fiducial" trajectory we are studying with the previous method.

Following notation [VTCP03], to find the Lyapunov exponent we calculate the biggest eigenvalue of the product

$$\prod_{k=0}^{n-1} T'_{n-k} E_{n-k} T_{n-k} P_{n-k}$$

for a big n (we used $n = 100000$); here T', R, T, P are the matrices giving the Jacobi fields at one iteration of the map 2.1. P gives the solution when the particle is inside the table Ω (no magnetic field); E when it is outside Ω (magnetic field B); T and T' when it is in the boundary transition, T for going out of Ω, T' for coming back inside.

$$P(t) = \begin{pmatrix} 1 & t \\ 0 & 1 \end{pmatrix}, \quad E(t) = \begin{pmatrix} \cos(Bt) & \frac{1}{B}\sin(Bt) \\ -B\sin(Bt) & \cos(Bt) \end{pmatrix}, \quad T(\theta) = \begin{pmatrix} 1 & 0 \\ B\arctan(\theta) & 1 \end{pmatrix}$$

Here θ is the corresponding angle of the particle with $\partial\Omega$ (see 2.2), and t is the time, since we are assuming constant speed 1, t could be interpreted as the distance traveled by the particle. Each of the matrices P, E, T are one-parameter subgroups of $SL(2, \mathbb{R})$.

Figure 4.7 shows the results of our calculations for the Lyapunov exponent after reducing the numerical noise; we plotted the more classical version of $r = \frac{1}{B}$ vs λ.

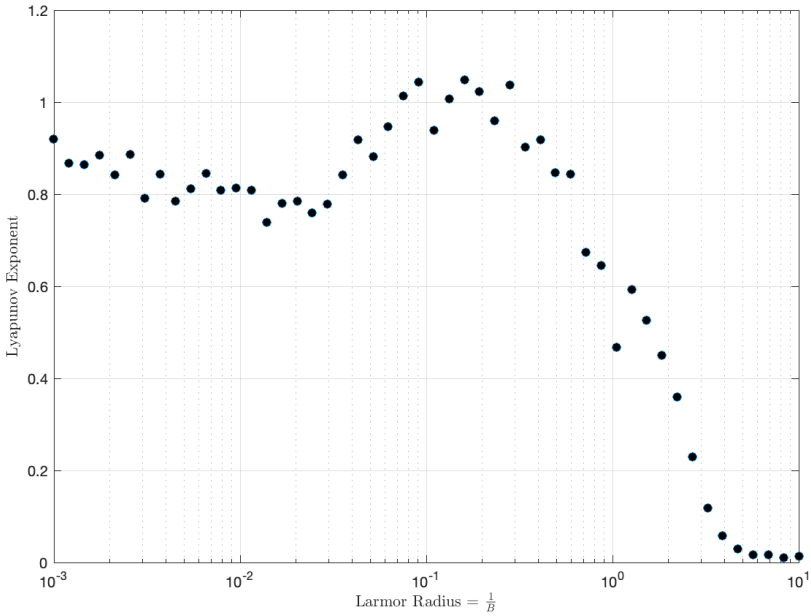

Figure 4.7: Lyapunov exponent for the inverse magnetic billiard system 1.1.2

In order to check our approach, we calculated the Lyapunov exponent with different “fiducial" trajectories with Wolf's method [WSSV85], and with the Jacobi Fields method. Figure 4.8 show three different cases that were used to reduce the numerical noise in order to obtain Figure 4.7.

The figures clearly show a correlation between the Lyapunov exponent λ and the strength of the magnetic field B. For small values of B, the value of λ is minimal. After $r > 5$, the system has a negligible Lyapunov exponent; this is because the orbits start to become circles with the square table as a point on them, see the Poincaré section and orbit examples in Figures 4.10 and 4.9.

Meanwhile, if B augments, so does λ. We can observe that λ grows significantly for $r < 0.3$ and doesn't come back down. This was also expected as we saw in the Poincaré sections that almost filled the whole phase space (see section

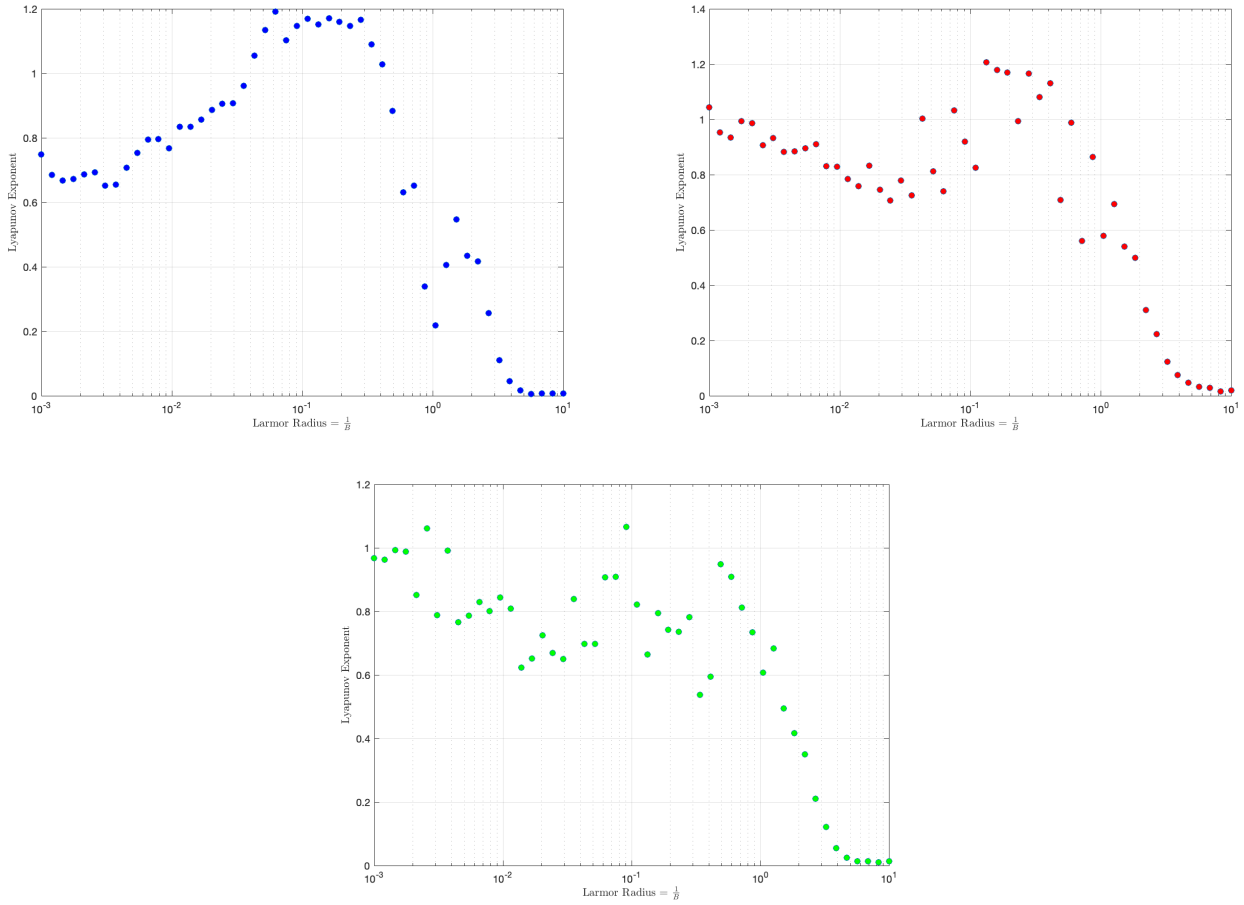

Figure 4.8: Lyapunov exponent for the inverse magnetic billiard system 1.1.2 with different "fiducial" trajectories.

4.1).

Notice that we have a peak at our calculations, and we do not have a smooth function as [VTCP03] with the Bunimovich billiard. We also have a discontinuity when $B \to \infty$, since our billiard table is integrable in the classical case, we have $\lambda = 0$, but in the figure we are not close to zero when B gets bigger.

We need to point out that ergodicity does not follow automatically from positive Lyapunov exponents.

Positive Lyapunov exponents for a billiard leads automatically to strong mixing properties: countable number of ergodic components, positive entropy, etc. [Woj86].

4.3 A note about Caustics

For classical billiards, if our billiard table Ω has curvature zero at some point of $\partial\Omega$, there exists no caustics for this problem. [Woj86] For the inverse magnetic problem can be proved that something similar happens (we will obtain parallel trajectories that can't be tangent to the same curve). [Gas21]
Our case has a difference: corners – our main obstruction since the beginning. But when the magnetic field is weak (r is big), the presence of corners have little to do with the dynamics of the problem. Numerically, our problem on the square behave similarly than the problem on the table consisting of a square with rounded corners by ϵ circles; and the same as the tables $x^{2n} + y^{2n} = 1$.
Having this in mind, it is surprising to see examples that show indication of the

existence of “caustics", that can be seen as an empty space, or as a cluttered hyperbolic region in the middle of the table that appear to be always tangent to the orbit.

The conjecture, more precisely, would be that for a radius big enough, there is an open set of initial conditions whose trajectories stay tangent to a continuous curve in the plane. Moreover, that there exist continuous curves that the billiard orbit is always tangent to.

We provide some examples that lead to this conjecture. This conjecture is supported by the Poincaré sections showed in4.1, and the ratio of regular to chaotic area showed in 4.6.

In some cases, this will lead to orbits not going through a disk at the center of the table. To illustrate, in table 4.1, we take $r \sim 2.1$, and a grid of initial conditions. Each row in the table represents a different initial position, each column a different initial velocity.

A similar result holds for radii big enough $r > 2$. This can be compared to the Poincaré sections and Lyapunov exponents calculated before. For bigger radii (small magnetic field) we have more regular space on Σ^2 and the chaos decreases – as seen in the Lyapunov exponent from before.

s \ $\tan\theta$	$\pi - 0.2$	$\pi - 0.1$	π	$\pi + 0.1$	$\pi + 0.2$
0.68	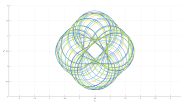	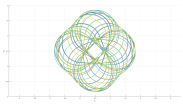	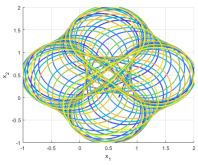	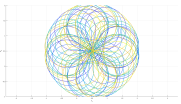	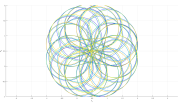
0.7	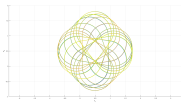	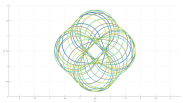		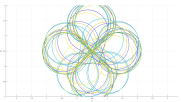	
0.8	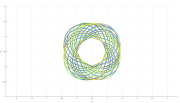	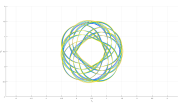	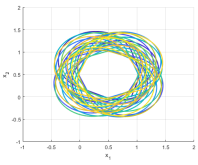	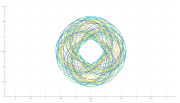	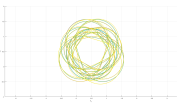
0.9	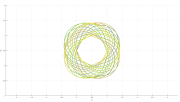	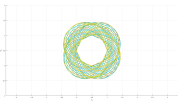	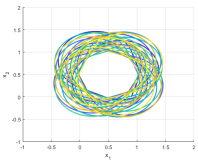	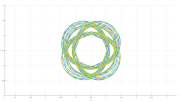	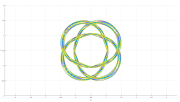
0.99	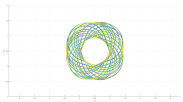	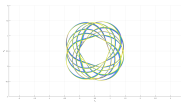	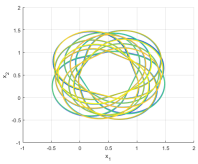	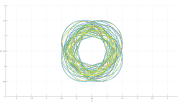	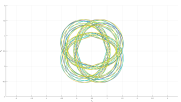

Table 4.1: Empty center

End Figure 4.9, shows an example of the empty center that we described, and it's Poincaré sections.

Figure 4.10, shows the case when the "caustic" is hyperbolic, and all the orbits get clustered in the center of the square.

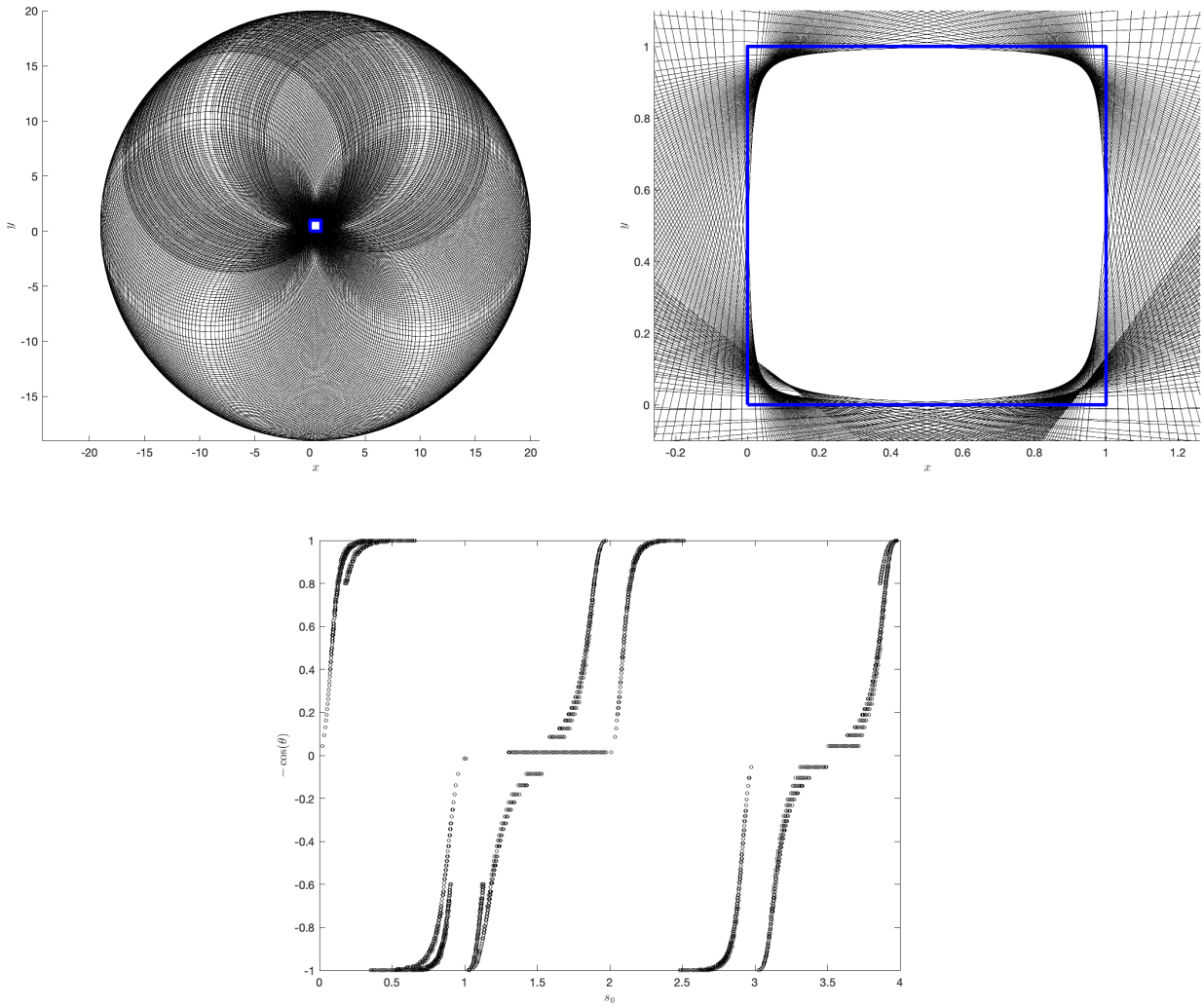

Figure 4.9: Orbit of $s = 0.9$, $\theta = 0.92$, $r = 10$, a close-up and its Poincaré section

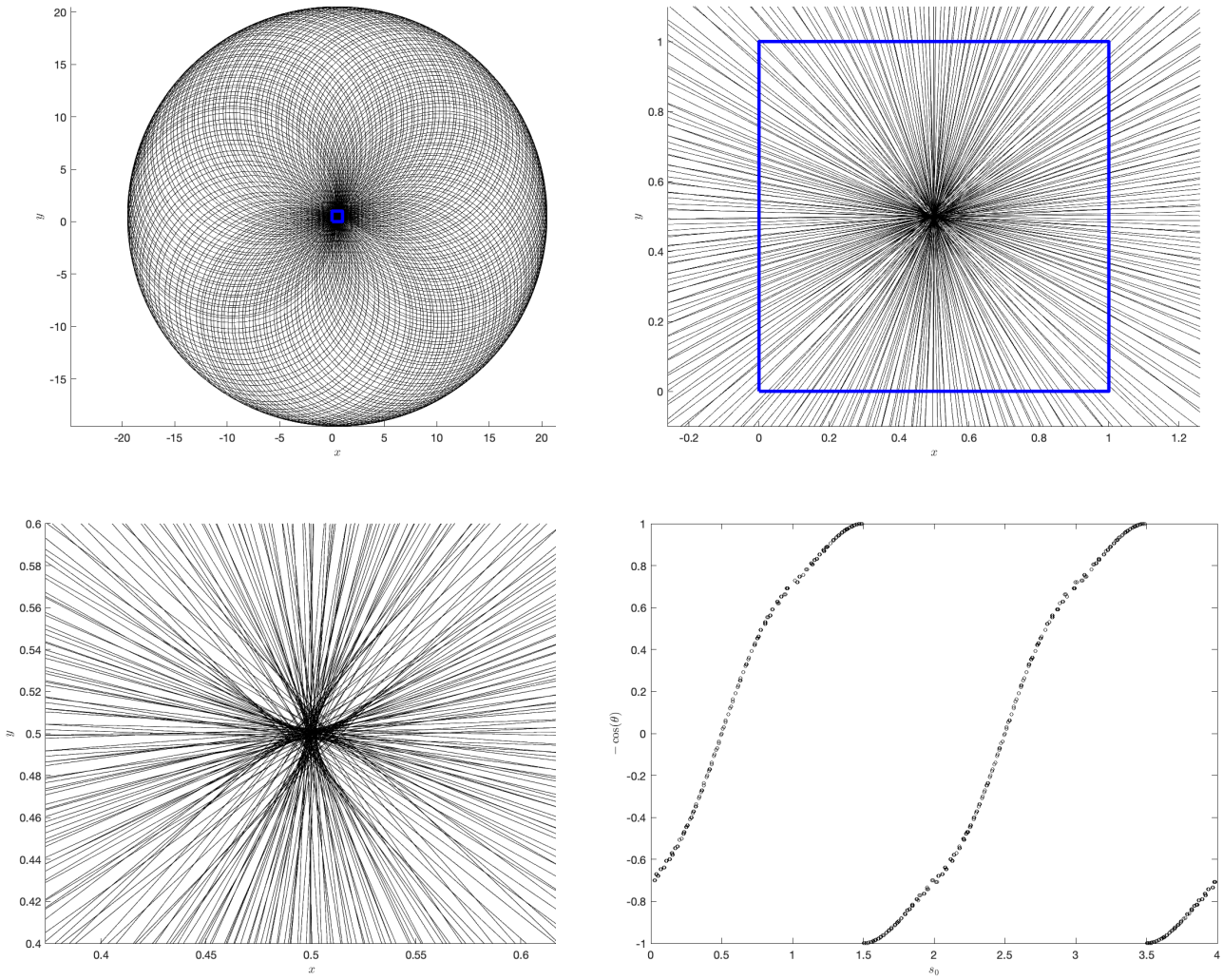

Figure 4.10: Orbit of $s = 0.5$, $\theta = \pi/2$, $r = 10$, two close-ups, and its Poincaré section.

Chapter 5

Conclusion + Next work

When the magnitude of the magnetic force goes to infinity, inverse magnetic billiard dynamics limits to classical billiards on the square, but turns out to be much more intricate and complicated than regular billiards. Numerical experiments and calculations suggest that the dynamics is ergodic for strong magnetic fields, while it has unexplained saw-tooth type patterns in the intermediate range of fields.

We proved the existence and partially classified periodic orbits with rational slopes that do not turn corners. The classification is not complete. Namely, we do not have specific conditions to get periodic orbits with slope different from p/q and $p+q$ odd.

We proved existence of periodic orbits for any given values of B and θ, Theorem 2 shows a dense set of these orbits for some conditions, see Example 3.3.1.

We calculated the Lyapunov exponent of the system, and found some dependence on the strength of the magnetic field. The surprise came on the jump that

is present when B goes to infinity, gong from positive to 0 (classical case).

There is much more to prove and see. Currently, we are working on the stability of periodic orbits - some recent work [Gas21] shows stability of a family of tables that limit to the square.

Bibliography

[Ami97] Edoh Amiran, *Integrable smooth planar billiards and evolutes*, New York Journal of Mathematics **3** (1997), 32–47.

[Arn78] V. I. Arnold, *Mathematical methods of classical mechanics*, Springer New York, 1978.

[AT18] Peter Albers and Serge Tabachnikov, *Introducing symplectic billiards*, Advances in Mathematics **333** (2018), 822–867.

[Bir27] G.D. Birkhoff, *Dynamical Systems*, American Mathematical Society / Providence, RI, American Mathematical Society, 1927.

[BK96] N. Berglund and H. Kunz, *Integrability and ergodicity of classical billiards in a magnetic field*, Journal of Statistical Physics **83** (1996), no. 1-2, 81–126.

[Bla16] W. Blaschke, *Kreis und Kugel*, zweite ed., Veit, 1916.

[Bun79] L. A. Bunimovich, *On the ergodic properties of nowhere dispersing billiards*, Communications in Mathematical Physics **65** (1979), no. 3, 295–312.

[Bun07] L. Bunimovich, *Dynamical billiards*, Scholarpedia **2** (2007), no. 8, 1813, revision #91212.

[Che88] Ping Chen, *Empirical and theoretical evidence of economic chaos*, System Dynamics Review **4** (1988), 81 – 108.

[CM06] Nikolai Chernov and Roberto Markarian, *Chaotic Billiards*, American Mathematical Soc., 2006.

[CP12] Giulio Casati and Tomaž Prosen, *Time Irreversible Billiards with Piecewise-Straight Trajectories*, Phys. Rev. Lett. **109** (2012), no. 17, 174101.

[DM15] Holger Dullin and Richard Montgomery, *Syzygies in the two center problem*, Nonlinearity **29** (2015).

[Dou82] Raphael Douady, *Applications du théoréme des tores invariants*, Ph.D. thesis, Université Paris VII, 1982.

[FLN+90] G.W. Frank, T. Lookman, M.A.H. Nerenberg, C. Essex, J. Lemieux, and W. Blume, *Chaotic time series analyses of epileptic seizures*, Physica D: Nonlinear Phenomena **46** (1990), no. 3, 427–438.

[Gas19] Sean Gasiorek, *On the dynamics of inverse magnetic billiards*, Ph.D. thesis, University of California Santa Cruz, (2019).

[Gas21] ———, *Linear stability of periodic trajectories in inverse magnetic billiards*, preprint, arXiv:2106.05676 (2021).

[Gol01] C. Golé, *Symplectic Twist Maps: Global Variational Techniques*, Advanced series in nonlinear dynamics, World Scientific, 2001.

[GP83] Peter Grassberger and Itamar Procaccia, *Estimation of the kolmogorov entropy from a chaotic signal*, Phys. Rev. A **28** (1983), 2591–2593.

[Hub87] Andrea Hubacher, *Instability of the boundary in the billiard ball problem*, Commun.Math. Phys. **108** (1987), no. 3, 483–488.

[KPC05] Bence Kocsis, Gergely Palla, and József Cserti, *Quantum and semiclassical study of magnetic quantum dots*, Physical Review B **71** (2005), no. 7, 075331.

[KROC08] A. Kormányos, P. Rakyta, L. Oroszlány, and J. Cserti, *Bound states in inhomogeneous magnetic field in graphene: Semiclassical approach*, Phys. Rev. B **78** (2008), no. 4, 045430.

[KS86] Anatole Katok and Jean-Marie Strelcyn, *Invariant manifolds, entropy and billiards: smooth maps with singularities*, Lecture notes in mathematics, no. 1222, Springer, Berlin, 1986, OCLC: 15018884.

[KS17] Andreas Knauf and Marcello Seri, *Symbolic dynamics of magnetic bumps*, Regul. Chaot. Dyn. **22** (2017), no. 4, 448–454.

[KSS13] Andreas Knauf, Frank Schulz, and Karl Friedrich Siburg, *Positive topological entropy for multi-bump magnetic fields*, Nonlinearity **26** (2013), no. 3, 727–743.

[KT91] V.V. Kozlov and D.V. Treshchëv, *Billiards: A Genetic Introduction to the Dynamics of Systems with Impacts: A Genetic Introduction to the Dynamics of Systems with Impacts*, Translations of Mathematical Monographs, American Mathematical Society, 1991.

[KZ18] Vadim Kaloshin and Ke Zhang, *Density of convex billiards with rational caustics*, Nonlinearity **31** (2018), no. 11, 5214–5234.

[Laz73] V F Lazutkin, *The Existence of Caustics for a Billiard Problem in a Convex Domain*, Mathematics of the USSR-Izvestiya **7** (1973), no. 1, 185–214.

[Mat82] John N. Mather, *Glancing billiards*, Ergodic Theory and Dynamical Systems **2** (1982), no. 3-4, 397–403.

[MBG93] O Meplan, F Brut, and C Gignoux, *Tangent map for classical billiards in magnetic fields*, J. Phys. A: Math. Gen. **26** (1993), no. 2, 237–246.

[Mei92] J. D. Meiss, *Symplectic maps, variational principles, and transport*, Reviews of Modern Physics **64** (1992), no. 3, 795–848.

[MF94] John N. Mather and Giovanni Forni, *Action minimizing orbits in hamiltomian systems*, Transition to Chaos in Classical and Quantum Mechanics: Lectures given at the 3rd Session of the Centro Internazionale Matematico Estivo (C.I.M.E.) held in Montecatini Terme, Italy, July 6-13, 1991 (Sandro Graffi, ed.), Springer Berlin Heidelberg, Berlin, Heidelberg, 1994, pp. 92–186.

[MH40] Marston Morse and Gustav A. Hedlund, *Symbolic dynamics ii. sturmian trajectories*, American Journal of Mathematics **62** (1940), no. 1, 1–42.

[Mos62] J. Moser, *On Invariant Curves of Area-preserving Mappings of an Annulus*, Nachrichten der Akademie der Wissenschaften in GÃ¶ttingen: II, Mathematisch-Physikalische Klasse, Vandenhoeck & Ruprecht, 1962.

[Mos16] _____, *Stable and Random Motions in Dynamical Systems: With Special Emphasis on Celestial Mechanics (AM-77)*, Princeton Landmarks in Mathematics and Physics, Princeton University Press, 2016.

[MRRTS16] Pau MartÃn, Rafael RamÃrez-Ros, and Anna Tamarit-Sariol, *On the length and area spectrum of analytic convex domains*, Nonlinearity **29** (2016), no. 1, 198–231.

[MT02] Howard Masur and Serge Tabachnikov, *Chapter 13 rational billiards and flat structures*, Handbook of Dynamical Systems, vol. 1, Elsevier Science, 2002, pp. 1015–1089.

[Nog10] Alain Nogaret, *Electron dynamics in inhomogeneous magnetic fields*, Journal of Physics: Condensed Matter **22** (2010), no. 25, 253201.

[RB85] M Robnik and M V Berry, *Classical billiards in magnetic fields*, J. Phys. A: Math. Gen. **18** (1985), no. 9, 1361–1378.

[RCD93] Michael T. Rosenstein, James J. Collins, and Carlo J. De Luca, *A practical method for calculating largest lyapunov exponents from small data sets*, Physica D: Nonlinear Phenomena **65** (1993), no. 1, 117–134.

[Rob86] Marko Robnik, *Regular and chaotic billiard dynamics in magnetic fields*, Nonlinear Phenomena and Chaos **1** (1986), 303–330.

[SG10] Yu Song and Yong Guo, *Bound states in a hybrid magnetic-electric quantum dot*, Journal of Applied Physics **108** (2010), no. 6, 064306.

[SIKL98] Heung-Sun Sim, G Ihm, N Kim, and S J Lee, *Magnetic Edge States in a Magnetic Quantum Dot*, Physical Review Letters **80** (1998), no. 7, 4.

[SLA12] J. Szücs, M. Levi, and V.I. Arnol'd, *Geometrical Methods in the Theory of Ordinary Differential Equations*, Grundlehren der mathematischen Wissenschaften, Springer New York, 2012.

[Sor18] A Sorrentino, *Some Computations*, Unpublished notes, 2018.

[SS85] M. Sano and Y. Sawada, *Measurement of the lyapunov spectrum from a chaotic time series*, Phys. Rev. Lett. **55** (1985), 1082–1085.

[Tab95] S. Tabachnikov, *Billiards*, Panoramas et synthèses - Société mathématique de France, Société mathématique de France, 1995.

[Tas97] Tamás Tasnádi, *Hard chaos in magnetic billiards¶(on the euclidean plane)*, Communications in Mathematical Physics **187** (1997), no. 3, 597–621.

[TS05] S. Tabachnikov and Pennsylvania State University Mathematics Advanced Study Semesters, *Geometry and Billiards*, Student mathematical library, American Mathematical Society, 2005.

[VTCP03] Z. Vörös, T. Tasnádi, J. Cserti, and P. Pollner, *Tunable Lyapunov exponent in inverse magnetic billiards*, Physical Review E **67** (2003), no. 6, 065202.

[VWA97] K. Vogtmann, A. Weinstein, and V.I. Arnol'd, *Mathematical Methods of Classical Mechanics*, Graduate Texts in Mathematics, Springer New York, 1997.

[Woj85] Maciej Wojtkowski, *Invariant families of cones and lyapunov exponents*, Ergodic Theory and Dynamical Systems **5** (1985), no. 1, 145–161.

[Woj86] ———, *Principles for the design of billiards with nonvanishing lyapunov exponents*, Communications in Mathematical Physics **105** (1986), no. 3, 391–414.

[WSSV85] Alan Wolf, Jack B. Swift, Harry L. Swinney, and John A. Vastano, *Determining lyapunov exponents from a time series*, Physica D: Nonlinear Phenomena **16** (1985), no. 3, 285–317.